iScience

CellPress
OPEN ACCESS

Article

# Genome-wide CRISPR-Cas9 screens identify mechanisms of BET bromodomain inhibitor sensitivity

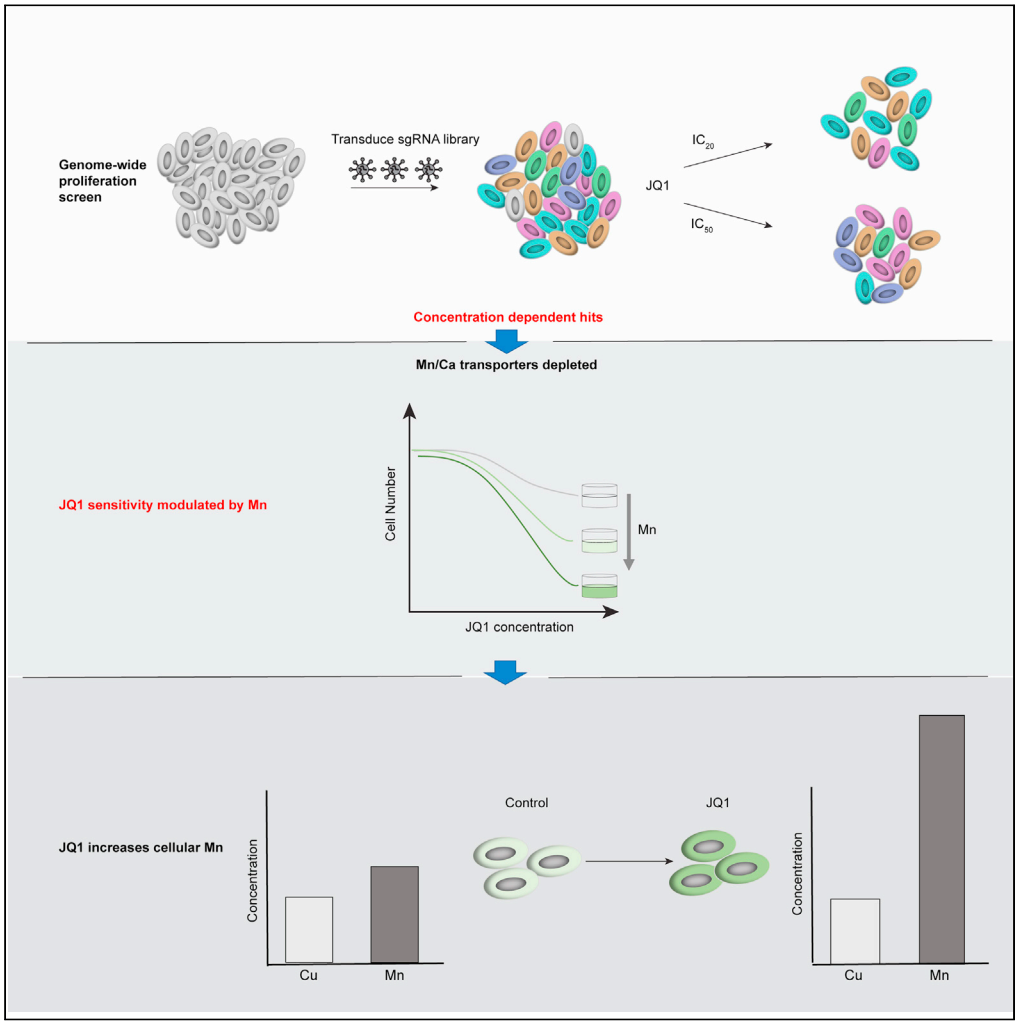


David Estoppey, Gabi Schutzius, Christian Kolter, ..., Tewis Bouwmeester, Dominic Hoepfner, Susan Kirkland

dominic.hoepfner@novartis.com (D.H.)
susan.kirkland@harvantispharma.co.uk (S.K.)

## Highlights

CRISPR screens identify genes regulating sensitivity to BET bromodomain inhibitors

Sensitivity and resistance hit lists are concentration-dependent

mTOR pathway mediates sensitivity to BET bromodomain inhibitors

Manganese regulates sensitivity to BET bromodomain inhibitors

Estoppey et al., iScience 24, 103323
November 19, 2021 © 2021 The Authors.
https://doi.org/10.1016/j.isci.2021.103323

iScience

CellPress
OPEN ACCESS

Article

# Genome-wide CRISPR-Cas9 screens identify mechanisms of BET bromodomain inhibitor sensitivity

David Estoppey,[1] Gabi Schutzius,[1,2] Christian Kolter,[1,2] Adrian Salathe,[1] Tiffany Wunderlin,[1] Amandine Meyer,[1] Florian Nigsch,[1] Tewis Bouwmeester,[1] Dominic Hoepfner,[1,3,*] and Susan Kirkland[1,*]

## SUMMARY

**BET bromodomain inhibitors hold promise as therapeutic agents in diverse indications, but their clinical progression has been challenging and none have received regulatory approval. Early clinical trials in cancer have shown heterogeneous clinical responses, development of resistance, and adverse events. Increased understanding of their mechanism(s) of action and identification of biomarkers are needed to identify appropriate indication(s) and achieve efficacious dosing. Using genome-wide CRISPR-Cas9 screens at different concentrations, we report molecular mechanisms defining cellular responses to BET inhibitors, some of which appear specific to a single compound concentration. We identify multiple transcriptional regulators and mTOR pathway members as key determinants of JQ1 sensitivity and two $Ca^{2+}$/$Mn^{2+}$ transporters, ATP2C1 and TMEM165, as key determinants of JQ1 resistance. Our study reveals new molecular mediators of BET bromodomain inhibitor effects, suggests the involvement of manganese, and provides a rich resource for discovery of biomarkers and targets for combination therapies.**

## INTRODUCTION

Bromodomain motifs mediate protein-protein interactions with acetylated lysine residues, a posttranslational modification with considerable physiological relevance (Ali et al., 2018). The BET family of proteins (BRD2, BRD3, BRD4, and BRDT) contain two bromodomains that have proved fruitful targets for the discovery of small molecule inhibitors (Cochran et al., 2019). BET proteins bind to acetylated histones at transcription start sites and regulate transcriptional co-activation and elongation via the formation of complexes containing RNA polymerase II, mediator, and pTEFb (Hajmirza et al., 2018). This feature of BET proteins has been particularly well described for BRD4, a key mediator of diverse physiological and pathological transcriptional responses including those seen in cancer (French, 2016; Marcotte et al., 2016).

Small molecule BET bromodomain inhibitors (BETi) mimic acetylated-lysine residues and regulate transcription by blocking BET protein binding to histone and nonhistone proteins (Shi and Vakoc, 2014). BETi are receiving increasing attention as potential therapeutics for diverse conditions including inflammatory, fibrotic, and cardiovascular disease (Duan et al., 2017; Jahagirdar et al., 2017; Lin and Du, 2020; Middleton et al., 2018) and have reached clinical studies for a variety of cancers (Amorim et al., 2016; Piha-Paul et al., 2019). However, these early trials have reported variable clinical responses, the development of resistance, and dose-limiting adverse events (Marcotte et al., 2016), which highlights the need for greater mechanistic understanding, alternative dosing regimens, and exploration of combination therapies (Alqahtani et al., 2019; Bechter and Schoffski, 2020). Questions remain as to why targeting BET proteins might benefit such a wide range of disease states and how BETi exposure relates to differential phenotypic and clinical outcomes (Kulikowski et al., 2020).

Chemogenomic screening provides a powerful and unbiased, genome-wide tool for dissecting molecular mechanisms regulating cellular responses to pharmacological agents. The CRISPR-Cas9 system significantly strengthens this approach by enabling genome-wide screening (Estoppey et al., 2017; Hoepfner et al., 2019) without the limitations of RNAi (Shalem et al., 2014). To uncover mechanisms mediating resistance or sensitivity to BETi, we performed genome-wide CRISPR-Cas9 screens in HCT116 colorectal cancer cells. To reveal any concentration-dependent molecular signaling, as suggested by other studies

[1]Novartis Institutes for Biomedical Research, Basel 4056, Switzerland

[2]These authors contributed equally

[3]Lead contact

*Correspondence: dominic.hoepfner@novartis.com (D.H.), susan.kirkland@harvantispharma.co.uk (S.K.)

https://doi.org/10.1016/j.isci.2021.103323


This is an open access article under the CC BY-NC-ND license (http://creativecommons.org/licenses/by-nc-nd/4.0/).

(Schutzius et al., 2021), we performed screening at two concentrations of JQ1 (Filippakopoulos et al., 2010). Our screens identify genes already known to mediate BETi sensitivity alongside many others not previously described such as the $Ca^{2+}/Mn^{2+}$ transporter, ATP2C1. Further validation of the ATP2C1 finding led us to discover a novel link between BETi effects and manganese biology, which warrants further exploration. Importantly, our data suggest that some molecular mechanisms responsible for BETi-induced changes in cell proliferation are concentration specific.

## RESULTS

### Genome-wide CRISPR-Cas9 screening identifies multiple mediators of BET bromodomain inhibitor sensitivity

Genome-wide CRISPR-Cas9 screening was performed in stable Cas9-expressing HCT116 cells (later referred to as HCT116-WT), which demonstrate efficient editing (Brodsky, 2009) (Figures S1A–S1C) and are near diploid, as gene copy number affects chemogenomics. The dose-dependent effect of JQ1 was established before chemogenomic screening, which requires careful dosing at sublethal concentrations (Figure S1D), then screens were performed in control medium, 0.2 μM JQ1 ($IC_{20}$) or 1 μM JQ1 ($IC_{50}$) (Figure 1A). To generate targeted loss-of-function alleles with genome-wide coverage we deployed a lentiviral single-guide RNA (sgRNA) library with a redundancy of 5 sgRNA/gene, multiplicity of infection around 0.5, and a coverage of 500 cells/sgRNA (Hoepfner et al., 2019). Cells were passaged after 8 and 12 days and then at 15 days we determined the frequency of individual sgRNAs in the resultant populations using next-generation sequencing of sgRNA amplified from genomic DNA. Raw sequencing reads were aligned using bowtie (Figures S2A and S2B). For gene-based hit calling, consistency of all sgRNAs per gene was considered and RSA (redundant sgRNA activity) calculated (Potting et al., 2018). A set of essential gene sgRNAs were included as an internal control, most of which were depleted in HCT116 untreated cells compared with plasmid (Figure S2C), confirming the quality of the data.

Comparing RSA p values of enriched and depleted sgRNAs between cells grown in JQ1 and control medium (Table S1), we showed that editing of 425 genes conferred JQ1 sensitivity (reduced cell proliferation) (Figure 1B; Table S2) and 396 genes conferred JQ1 resistance (increased cell proliferation) (Figure 1B; Table S3) in 1 μM JQ1. In addition, with 0.2 μM JQ1, editing of 314 genes conferred sensitivity (Figure 1B; Table S4) and 301 genes resistance (Figure 1B; Table S5). Importantly, most hits were exclusively observed in either 0.2 μM or 1 μM JQ1, with only a limited number of hits observed in both whole genome screens (56 genes conferring sensitivity versus 73 genes conferring resistance) (Figure 1B). For example, ATP2C1 was a sensitizing hit in both screens, whereas KEAP1 and SQSTM1 were sensitizing hits restricted solely to the 1 μM or 0.2 μM screens, respectively (Figure 1B). Among resistance-inducing hits we observed ATP6AP2 in both screens, whereas LAMTOR2 and RPAP1 were hits restricted to 1 μM or 0.2 μM screens, respectively. These concentration-specific hit lists with JQ1 were not seen in previous LMW CRISPR-Cas9 screens (Estoppey et al., 2017), supporting the idea that JQ1 exerts some dose-dependent biological effects through differential molecular drivers. This was further supported by gene set enrichment analysis, which only identified enriched gene sets among hits of the 1 μM but not the 0.2 μM JQ1 screen. In 1 μM JQ1, sgRNAs that were specifically depleted included those associated with transcriptional regulation from RNA polymerase II promoter (Figures 1C, 1D, and 2A) and protein deubiquitination, indicating the importance of these pathways in maintaining proliferation under bromodomain inhibition. Conversely, sgRNAs that were specifically enriched after 1 μM JQ1 treatment included those associated with mTOR signaling, cardiolipin metabolism, and MAPKK activation (Figures 1C, 1D, and 2A), indicating that targeting these pathways rendered cells more resistant to bromodomain inhibition.

Our screen identified previously described genes whose editing confers BETi sensitivity such as transcriptional regulators (Figure 1D) (Shu et al., 2020) and those whose editing conferred BETi resistance such as SPOP (Figure 2B, right panel). SPOP mutations are shown to increase BETi resistance by stabilizing BRD4 (Dai et al., 2017) but no BET proteins were among our resistance hits (Figure 2B, right panel). SPOP is a component of the CUL3 ubiquitin ligase complex and interestingly we found that sgRNAs for CUL3 itself and KEAP1, another of its adapter proteins, were highly depleted in 1 μM JQ1 screen (Figure 2B, left panel), suggesting that their substrate protein(s) promotes BETi sensitivity. BETi-modulated ubiquitination was further suggested, as sgRNAs to USP16, a deubiquitinating enzyme that targets histone H2A and regulates stem cell function, and HECTD1, a ubiquitin E3 ligase, were enriched in 1 μM JQ1 treated cells (Table S3). Notably, HECTD1 depletes the EMT-inducing transcription factor SNAIL (SNAI1) (Wang et al., 2020), whereas CTDSPL2, a phosphatase opposing degradation of SNAIL and promoting EMT

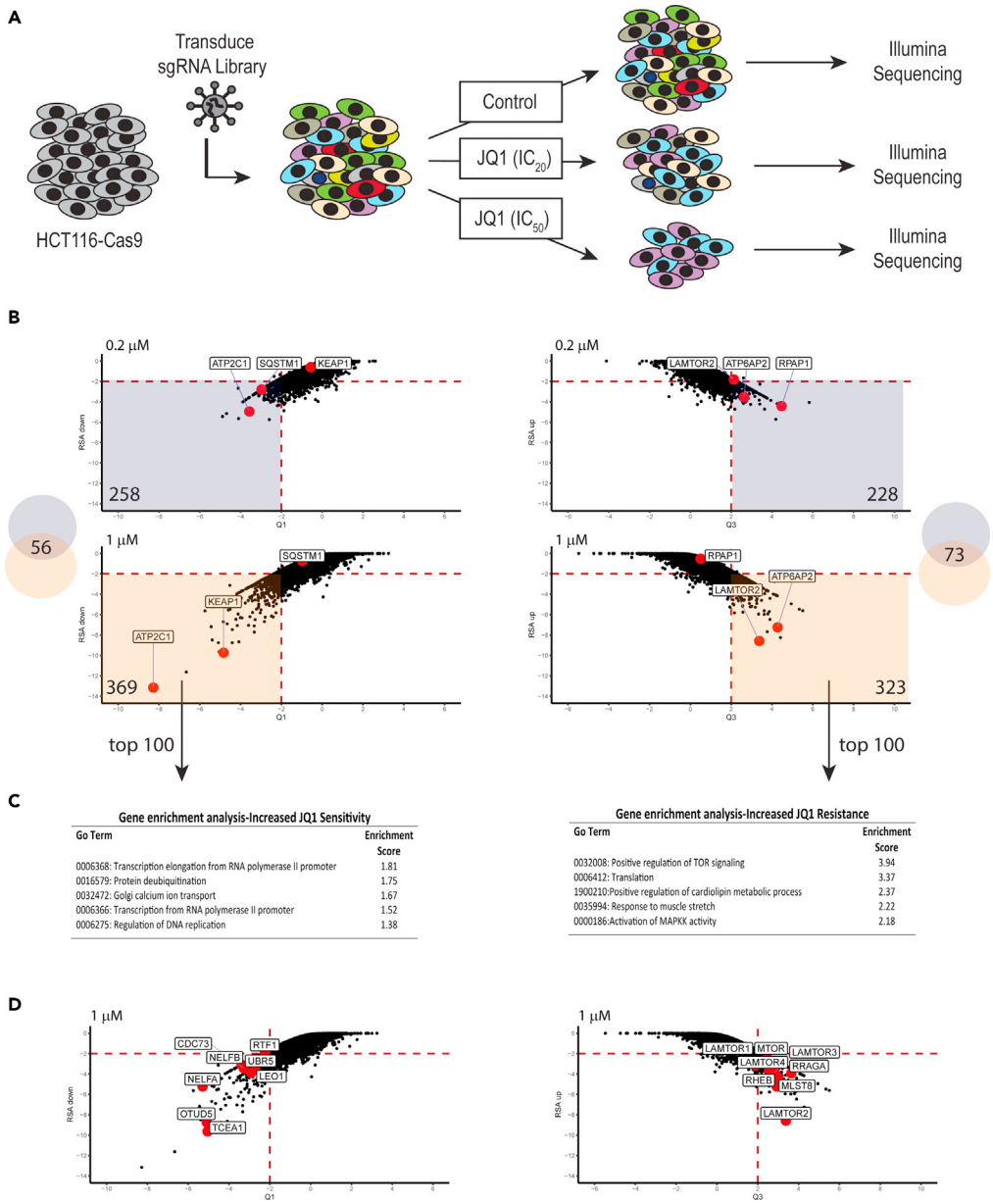


**Figure 1. Genome-wide CRISPR-Cas9 screen identifies genes mediating BETi sensitivity**

(A) Schematic workflow for the whole genome CRISPR-Cas9 screen in HCT116 cells.

(B) Significant hits of genes whose editing imposed sensitivity (depletion of sgRNAs) (left panels). Three hundred fourteen genes in 0.2 μM JQ1 (top left panel) and 425 genes in 1 μM JQ1 (bottom left panel). Fifty-six of those sensitivity hits were found in both 0.2 μM and 1 μM JQ1 screens. Significant hits of genes whose editing imposed resistance (enrichment of sgRNAs) (right panels). Three hundred one genes in 0.2 μM JQ1 (top right panel) and 396 genes in 1 μM JQ1 (bottom right panel). Seventy-three of those resistance hits were found in both 0.2 μM and 1 μM JQ1 screens. The graph plots of screening data show RSA p value (a gene-level measure for conserved depletion of its respective guides) against Q1/3 (a gene level effect size corresponding to the RSA p value).

(C) Gene set enrichment for the top 100 genes imposing sensitivity (left) or resistance (right) in 1 μM JQ1.

(D) Top hits representing genes within the most significant gene set imposing sensitivity "Transcription elongation from RNA polymerase II promoter" (left plot) and resistance "Positive regulation of TOR signaling" (right plot) in 1 μM JQ1

(Zhao et al., 2018), was among the top sensitizing hits (Figure 2B, left panel, and Table S2). SNAIL itself was depleted in 1 μM JQ1 (Q1: −1.69 and RSA DOWN: −1.3) but below our thresholds (Q1: −2 and RSA DOWN: −2) and therefore not among hits.

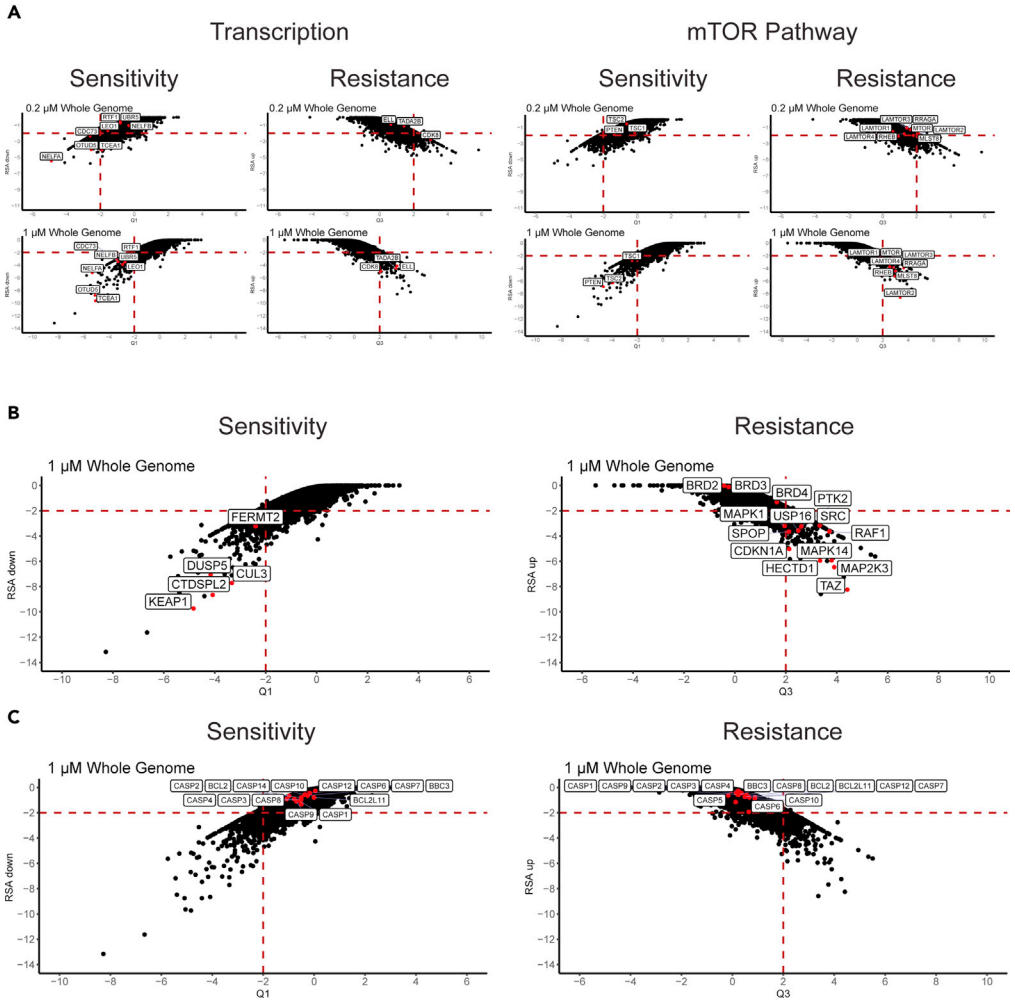


**Figure 2. Whole genome screening hits mediating sensitivity or resistance to JQ1**

(A) Genes identified as hits, which form part of the two most significant gene enrichments from the 1 μM JQ1 whole genome screen. Transcription (left hand panels) genes from "Transcriptional elongation from RNA polymerase II promoter" which score as sensitivity or resistance hits in 0.2 μM JQ1 (top panels) or 1 μM JQ1 (lower panels). mTOR pathway-right hand panels, genes from "Positive regulation of TOR signaling" which score as sensitivity or resistance hits in 0.2 μM JQ1 (top panels) or 1 μM JQ1 (lower panels).

(B) Genes whose editing imposes increased sensitivity (left panel) or resistance (right panel) to the inhibition of cell proliferation by 1 μM JQ1. BRD2, BRD3, and BRD4 are shown in right panel.

(C) Key apoptosis mediators (BBC3, BCL2L1, BCL2, multiple caspases) are not hits in1 μM JQ1.

BETi effects appear generally cytostatic (Ma et al., 2017) but some reports describe apoptosis. Cell-cycle arrest in $G_1$ is associated with increased expression of CDKN1A (p21) (Ma et al., 2017), a resistance hit in our 1 μM screen (Figure 2B, right panel, Table S3) and in another JQ1 screen (Shu et al., 2020). In contrast, key apoptosis mediators (BBC3, BCL2L1, BCL2, multiple caspases) were not hits, (Figure 2C) suggesting that apoptosis was not induced in HCT116 cells even after sustained growth in 1 μM JQ1.

## Mechanisms mediating sensitivity to JQ1 (resistance screening hits)

### *mTOR pathway*

The mechanistic target of rapamycin (mTOR) pathway, via mTORC1 and mTORC2 complexes, regulates diverse metabolic processes. When amino acids are abundant, mTORC1 associates with Rag GTPases and the Ragulator complex and translocates to the lysosomal membrane (Sancak et al., 2010). Our screen revealed that editing of multiple genes associated with mTORC1 biology led to JQ1 resistance including members of the mTORC1 (mTOR, MLST8) and Ragulator complexes (LAMTOR1, LAMTOR2, LAMTOR3,

LAMTOR4) alongside activators of mTORC1 (RRAGA and RHEB) (Figures 1D and 2A). In contrast, editing of negative regulators (PTEN, TSC1, TSC2) induced sensitivity to JQ1 (Figure 2A), suggesting that BETi reduce HCT116 proliferation by hyperactivating mTOR signaling, which has previously been associated with senescence induction (Astle et al., 2012). Of note, these mTOR related hits were not found in 0.2 μM JQ1, suggesting that mTOR signaling only reaches levels sufficient to reduce cell proliferation at higher concentrations of BETi.

### *MAPK pathways*

Gene enrichment implicated MAPK pathways as mediators of BETi effects (Figure 1C). MAPK14 (p38) and its regulator MAP2K3 were robust resistance hits (Figure 2B), suggesting that enhanced p38 signaling, again potentially via senescence induction (Xu et al., 2014), reduces proliferation. In addition, editing of positive regulators of ERK signaling (SRC, RAF1, PTK2 [FAK]) increased JQ1 resistance, whereas editing of DUSP5, a negative regulator (Kidger et al., 2017), increased JQ1 sensitivity (Figure 2B). MAPK1 (ERK) was depleted but just below significance (Q2: 1.95 and RSA UP: −3.2). As MAPK hits were only seen at 1 μM JQ1, it suggested that a certain level of activation was needed to reduce proliferation, which is consistent with studies showing that hyperactivation of MAPK signaling is deleterious to RAS/Raf mutant cells such as HCT116 ($Kras^{G13D}$) (Leung et al., 2019). In this context, our finding that DUSP5 editing increased BETi sensitivity warrants further investigation.

### *Cardiolipin metabolism*

Our screen further linked BETi effects to cardiolipin, a phospholipid regulator of mitochondrial function (Wasmus and Dudek, 2020), as Tafazzin (TAZ), a transacylase that remodels cardiolipin, and other hits, OPA1 and STOML2 with links to cardiolipin function, were among resistance hits (Figure 2B; Table S3). Defective cardiolipin remodeling is linked to inherited disease such as Barth syndrome caused by Tafazzin mutations (Wasmus and Dudek, 2020).

## Mechanisms increasing resistance to JQ1 (sensitivity screening hits)

### *Transcriptional regulators*

BRD4 regulates transcription, DNA damage response, and genome integrity (Donati et al., 2018; Zhang et al., 2018). Hypersensitivity to 1 μM JQ1 resulted upon loss of RNA polymerase complex components (NELFA, NELFB, LEO1, CDC73, RTF1) (Core and Adelman, 2019; Xu et al., 2017) or genes regulating DNA damage response or genome stability (OTUD5, UBR5, and TCEA-1) (Figures 1D and 2A) (Zatreanu et al., 2019), whereas editing of TADA2B, ELL, and CDK8, components of the SAGA (Helmlinger and Tora, 2017), SEC (Knutson et al., 2016), and Mediator (Menzl et al., 2019) complexes, respectively, (Figure 2A; Table S3) increased JQ1 resistance. Interestingly, CDK8 inhibitors have been shown both to increase mediator recruitment to RNA polymerase II (RNA Pol II) and to confer resistance to BETi (Lynch et al., 2020). In contrast, the 0.2 μM JQ1 resistance hit list contains few transcriptional regulators (Figure 2A) but uniquely and notably contains RPAP1, an important regulator of mediator driven transcription and cell identity (Figure 1B) (Lynch et al., 2018). The findings suggest a complex, concentration-dependent transcriptional response to JQ1.

### *$Mn^{2+}$/$Ca^{2+}$ ion transporters*

An intriguing finding in both screens was the sensitizing effect of editing ATP2C1 (SPCA1), a $Ca^{2+}$/$Mn^{2+}$ transporter responsible for maintaining intracellular calcium and manganese homeostasis (Xia et al., 2017) (Figure 1B). Mutations in ATP2C1 result in abnormal cytosolic $Ca^{2+}$/$Mn^{2+}$ levels and manifest clinically as Hailey-Hailey disease (Deng and Xiao, 2017). Notably, TMEM165, a second Golgi located $Ca^{2+}$/$Mn^{2+}$ transporter, was found among sensitizing hits in both screens (Tables S2 and S4). TMEM165 also regulates manganese homeostasis (Colinet et al., 2016; Potelle et al., 2016), further implicated manganese or calcium in JQ1 responses. This possibility was investigated after validation of the screens.

## Validation of whole genome CRISPR-Cas9 screen

### *Mini-pool CRISPR-Cas9 screen*

To evaluate the reproducibility and specificity of screening data we performed an independent screen using 547 genes in HCT116 cells grown in either 1 μM JQ1 or 1 μM JQ1 (−), its inactive enantiomer (Table S6). The mini-pool screen using 1 μM JQ1 confirmed 21 out of 24 genes increasing sensitivity and 19 of 21 inducing resistance previously found in the whole genome screen using 1 μM JQ1 (Figure 3A; Tables S7 and S8). Such reproducibility further supported the quality of our CRISPR screening data. By applying an

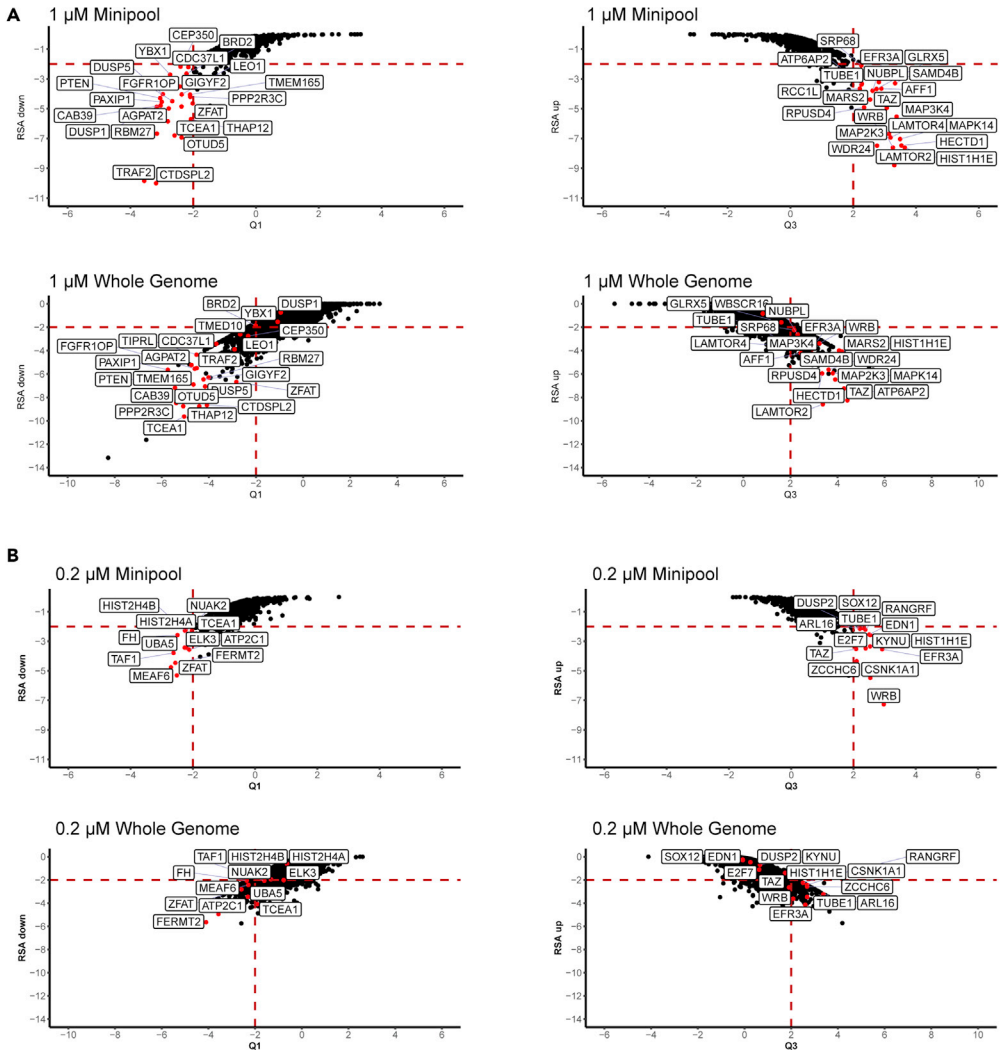


**Figure 3. Comparison whole genome and repeat mini-pool JQ1 screen**

(A) Comparison of hits identified as imposing sensitivity or resistance to JQ1 in a whole genome CRISPR-Cas9 screen (bottom panels) and an independent "mini-pool" screen (Top panels) using 1 μM JQ1. Red dots highlight significant hits from the "mini-pool."

(B) Comparison of hits identified as imposing sensitivity or resistance to JQ1 in a whole genome CRISPR-Cas9 screen (bottom panels) and an independent "mini-pool" screen (Top panels) using 0.2 μM JQ1. Red dots highlight significant hits from the "mini-pool."

additional filter (inactive enantiomer (JQ1 (−)) we showed that most hits (except HIST1H1E and SAMD4B [Table S6]) were exclusively seen with JQ1 treatment supporting the selectivity of our screen. Moreover, we performed an additional independent mini-pool screen using 0.2 μM JQ1, which confirmed 6 out of 12 genes increasing sensitivity and 7 of 14 inducing resistance previously found in the whole genome screen using 0.2 μM JQ1 (Figure 3B; Tables S9, S10, and S11). These findings indicate a decreased reproducibility of hits in 0.2 μM JQ1 and furthermore show that reproducible hits tended to be those such as ATP2C1 previously seen in both 1 μM and 0.2 μM JQ1 whole genome screens (e.g. 5 out of 6 genes increasing sensitivity are hits for 0.2 and 1 μM JQ1 in the whole genome screen; and 5 out of 7 genes increasing resistance are hits for 0.2 and 1 μM JQ1 in the whole genome screen). The reduced number and significance of hits in the lower concentration of JQ1, as seen with other LMW CRISPR-Cas9 screens (Estoppey et al., 2017), seems likely to contribute to this apparent reduction in reproducibility. Nevertheless, we still observe genes such as UBA5, which is a confirmed sensitivity hit in 0.2 μM JQ1 but not in 1 μM JQ1 (Figures 3A and 3B). Further comparison of our 0.2 μM screening data with publicly available datasets

(Shu et al., 2020) (Figure S3A) shows that UBA5 is also a sensitivity hit to JQ1 in SUM149 cells, clustering close to FERMT2 and ATP2C1 (Shu et al., 2020). By contrast, BRD2 was among the top sensitivity hits in this publicly available dataset (Shu et al., 2020) but not found as a sensitivity hit in our 0.2 μM screen although it was a confirmed sensitivity hit in both 1 μM JQ1 screens (Figures S3A and S3B). Interestingly, OTUD5 was a specific hit in both of our screens for the high concentration but did not score for sensitivity in the SUM149 cells (Figure S3B) (Shu et al., 2020). In conclusion, this suggests that in addition to concentration dependent effects, further cell-line-specific effects influence sensitivity to BET inhibitors.

### *CRISPR-Cas9 editing of ATP2C1, DUSP5, or FERMT2 increases JQ1 sensitivity*

To further validate the results, we edited HCT116-**WT** cells using CRISPR-Cas9 with a single sgRNA to sensitizing hits, ATP2C1, DUSP5, and FERMT2. Clones were derived from each edited population, designated HCT116-**ATP2C1,** HCT116-**DUSP5**, and HCT116-**FERMT2**, and editing confirmed by genotyping (Figures S4A and S4B). We further characterized the HCT116-**ATP2C1** cells and showed that ATP2C1 protein (Figure S4C) and mRNA (Figure S4D) were significantly reduced compared with HCT116-**WT** cells. Although HCT116-**ATP2C1**, HCT116-**DUSP5**, and HCT116-**FERMT2** showed similar growth rates to HCT116-**WT** cells in control medium (Figure 4A), they all showed significantly slower growth than wild-type cells when grown in 0.3125, 1.25, and 5 μM JQ1 (Figure 4A), confirming our screening data.

Although FERMT2 (Kindlin-2), a regulator of integrin signaling (Sossey-Alaoui et al., 2019), protects cells from growth inhibition by JQ1, other mediators of integrin signaling (PTK2, MAPK1, RAF1, SRC [Fang et al., 2018]) conferred sensitivity to JQ1 (Table S1, Figure 2B, right panel) suggesting that other FERMT2 functions, such as proline synthesis regulation (Guo et al., 2019), may contribute to BETi resistance.

DUSP5, a phosphatase inhibitor of ERK1/2 kinases, acted synergistically with JQ1, suggesting that hyperactivated ERK signaling slows growth in BETi and supporting further investigation of DUSP5 as a potential target for combination therapy.

Finally, we show that the loss of ATP2C1 acted synergistically with JQ1 to further reduce HCT116 proliferation when compared with HCT116-**WT** cells (Figure 4A). Dose response studies showed that HCT116-**ATP2C1** cells were significantly more sensitive ($IC_{50}$ = 0.34 μM) to JQ1 than HCT116-**WT** cells ($IC_{50}$ = 0.64 μM) (Figure 4B) but not to Paclitaxel, a clinical chemotherapeutic agent (Tsimberidou et al., 2011; Wang et al., 2017) (Figure 4C). Similarly, we found no increased sensitivity to Paclitaxel with HCT116-**DUSP5** or HCT116-**FERMT2** cells compared with the HCT116-**WT** cells (Figure 4C), suggesting that loss of these proteins had not generally sensitized cells to all chemotherapeutic agents.

## Extracellular manganese, but not calcium, concentration regulates sensitivity to JQ1

In addition to ATP2C1, our screens identified a second Golgi-located $Ca^{2+}/Mn^{2+}$ transporter, TMEM165 (Colinet et al., 2016), among the sensitizing hits (Figure 5A). Loss of either ATP2C1 or TMEM165 had no effect on cell proliferation in control medium but significantly reduced proliferation with JQ1 (Figure 5A). This led us to further investigate a potential role for $Ca^{2+}/Mn^{2+}$ ions in cellular responses to BETi. We asked whether extracellular calcium or manganese concentration influenced the antiproliferative effect of BETi and showed that increasing $Ca^{2+}$ levels using $CaCl_2$ by 15 μM, 30 μM, or 60 μM had no effect on growth in untreated, JQ1- or JQ1 (−)-treated HCT116-**WT** cells (Figure 5B). Dose responsive inhibition of HCT116 cell growth with OTX015, another BET inhibitor, was also unchanged with increasing concentrations of extracellular $CaCl_2$ (Figure 5B). Because manganese is cytotoxic at high concentrations, we carefully selected physiologically relevant manganese concentrations (Bowman and Aschner, 2014; Kumar et al., 2014) and importantly only included data from $MnCl_2$ concentrations that did not affect HCT116-**WT** growth. In contrast to the calcium data, JQ1 sensitivity of HCT116-**WT** cells ($IC_{50}$ 0.64 μM) was slightly increased at 30 μM $MnCl_2$ ($IC_{50}$ 0.53 μM) and significantly increased at 60 μM $MnCl_2$ ($IC_{50}$ 0.29 μM) (Figure 5C). Growth inhibition of HCT116 cells by OTX015 ($IC_{50}$ 2.43 μM) was similarly increased when extracellular manganese was raised to 15 μM $MnCl_2$ ($IC_{50}$ 1.9 μM), 30 μM $MnCl_2$ ($IC_{50}$ 1.16 μM), or 60 μM $MnCl_2$ ($IC_{50}$ 0.41) (Figure 5C).

We next investigated whether extracellular manganese influenced BETi sensitivity in other cells. We showed that increasing extracellular manganese increased sensitivity to JQ1 in HT-29 cells, colorectal cancer cells, from $IC_{50}$ 0.24 μM in untreated cells to $IC_{50}$ 0.12 μM in 60 μM $MnCl_2$ and 0.09 μM in 80 μM $MnCl_2$ (Figure 5D). Likewise, JQ1 inhibited the growth of SUM159 breast cancer cells with $IC_{50}$ 0.33 μM in untreated cells, $IC_{50}$ 0.13 μM in 60 μM $MnCl_2$ and $IC_{50}$ 0.09 μM in 80 μM $MnCl_2$ (Figure 5E).

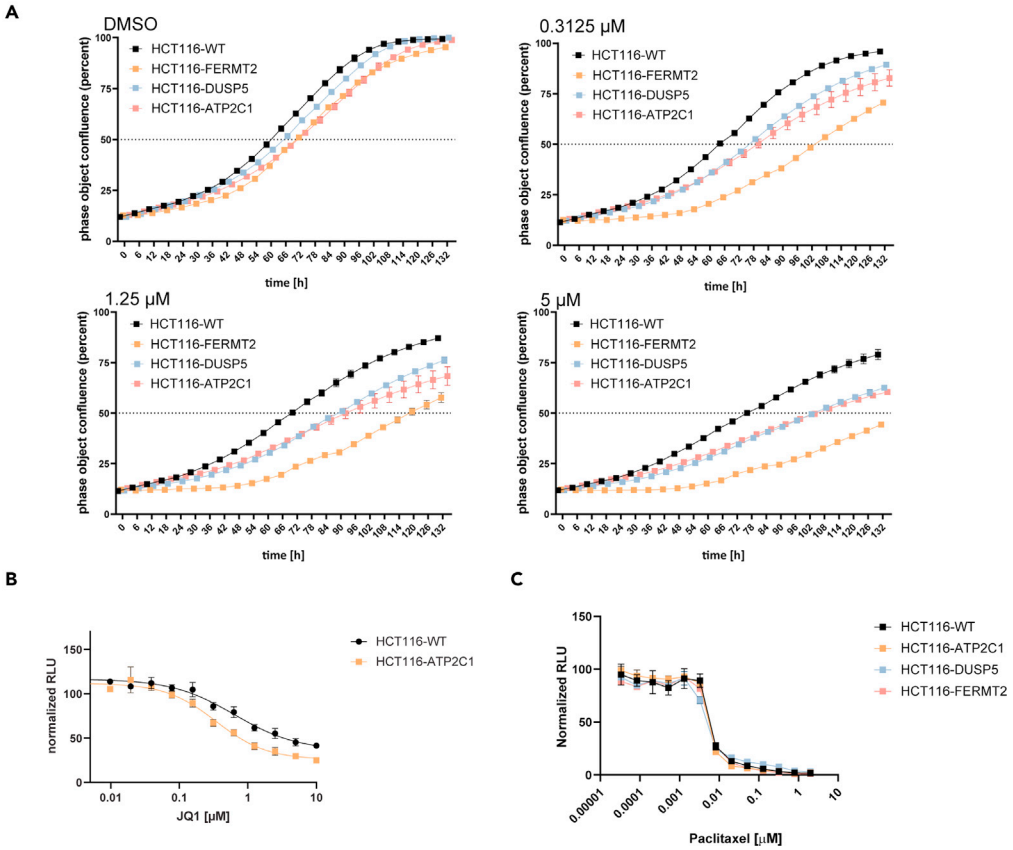


**Figure 4. Validation of whole-genome JQ1 sensitivity screen**

(A) Growth of HCT116-**WT**, HCT116-**ATP2C1**, HCT116-**DUSP5**, and HCT116-**FERMT2** in the presence of control medium or medium supplemented with JQ1 using the IncuCyte ZOOM live cell imaging system over 132 h. Cell growth is displayed as phase object confluence (percent) analyzed with the IncuCyte ZOOM Basic Analyzer.

(B) Dose response of JQ1 on cell proliferation of HCT116-**WT** and HCT116-**ATP2C1** cells. Cell number is measured using the CellTiter-Glo luminescence assay. Luminescence values are normalized to 100% in control medium to enable comparison between different cell lines. Mean ± S.D. (n = 3).

(C) Dose response of Paclitaxel on cell proliferation of HCT116-**WT**, HCT116-**ATP2C1**, HCT116-**DUSP5**, and HCT116-**FERMT2** cells. Luminescence values are normalized to 100% in control medium to enable comparison between different cell lines. Mean ± S.D. (n = 3)

As HCT116-**ATP2C1** cells showed an inherent increased sensitivity to JQ1, we asked whether these cells were more susceptible to the additional effects of increased calcium or manganese. HCT116-**ATP2C1** cells showed a significant increased JQ1 sensitivity when manganese levels were increased in the culture medium. Compared with the small effect on JQ1 sensitivity seen in wild-type cells grown at 30 µM $MnCl_2$, HCT116-**ATP2C1** cells showed a 7-fold increase in JQ1 sensitivity when grown in 30 µM $MnCl_2$ ($IC_{50}$ 0.045 µM) compared with no $MnCl_2$ ($IC_{50}$ 0.34 µM) (Figure 5F). In contrast, the sensitivity of HCT116-**ATP2C1** cells was unchanged with increasing calcium levels (Figure 5G) as seen with the HCT116-**WT** cells.

Our data show that extracellular manganese and ATP2C1 regulate the sensitivity of cells to BETi, strongly suggesting a link to manganese biology. Whether these effects are mediated by BRD4 transcriptional control of manganese homeostasis remains to be determined although there is no significant change in ATP2C1 protein expression after 24 h of JQ1 treatment (Figure S5).

## BET inhibitors increase intracellular manganese concentration in colorectal cancer cells

As increasing extracellular manganese concentration increased sensitivity to JQ1, we asked whether BETi modulated intracellular manganese levels using an optimized cellular Fura-2 manganese extraction assay (CFMEA) as described (Kumar et al., 2014; Kwakye et al., 2011). CFMEA uses the ability of $Mn^{2+}$ to quench

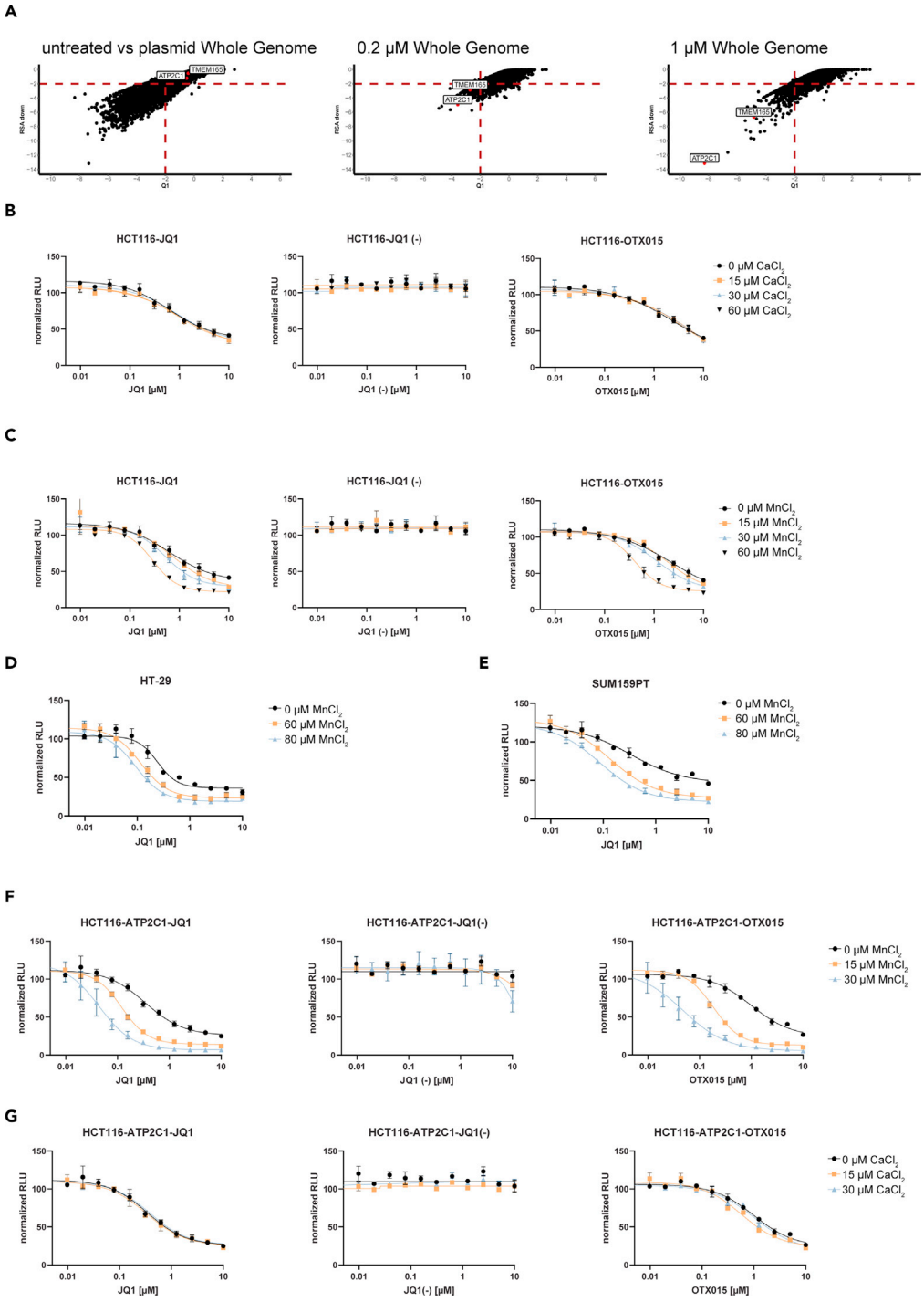


**Figure 5. Manganese modulates cellular sensitivity to JQ1**

(A) Genome wide CRISPR-Cas9 screen profiles highlighting ATP2C1 and TMEM165, in HCT116-**WT** cells. The left panel shows the relative abundance of ATP2C1 and TMEM165 sgRNAs compared with the initial library. The next two panels show the relative abundance of ATP2C1 and TMEM165 sgRNAs upon JQ1 treatment at $IC_{20}$ (0.2 μM) (middle panel) and $IC_{50}$ (1 μM) (right panel) compared with untreated cells.

(B) Dose response effects of JQ1, JQ1 (–), or OTX015 on cell proliferation of HCT116-**WT** cells in the presence of different concentrations of $CaCl_2$. Luminescence values are normalized to 100% in control medium to enable comparison between different cell lines. Mean ± S.D. (n = 3).

**Figure 5. *Continued***

(C) Dose response of JQ1, JQ1 (−), or OTX015 on cell proliferation of HCT116-**WT** cells in the presence of different concentrations of $MnCl_2$. Luminescence values are normalized to 100% in control medium to enable comparison between different cell lines. Mean ± S.D. (n = 3).

(D) Dose response of JQ1 on cell proliferation of HT-29 **cells** in the presence of different concentrations of $MnCl_2$. Luminescence values are normalized to 100% in control medium to enable comparison between different cell lines. Mean ± S.D. (n = 3).

(E) Dose response of JQ1 on cell proliferation of SUM159PT cells in the presence of different concentrations of $MnCl_2$. Luminescence values are normalized to 100% in control medium to enable comparison between different cell lines. Mean ± S.D. (n = 3).

(F) Dose response of JQ1, JQ1 (−), and OTX015 on cell proliferation of HCT116-**ATP2C1** cells in the presence of different concentrations of $MnCl_2$. (Luminescence values are normalized to 100% in control medium to enable comparison between different cell lines. Mean ± S.D. (n = 3).

(G) Dose response of JQ1, JQ1 (−), and OTX015 on cell proliferation of HCT116-**ATP2C1** cells in the presence of different concentrations of $CaCl_2$. (Luminescence values are normalized to 100% in control medium to enable comparison between different cell lines. Mean ± S.D. (n = 3).

Fura-2 fluorescence and gives an accurate assessment of extracted $Mn^{2+}$ levels over a range of 0.1–10 μM. JQ1 dose-dependently increased intracellular $Mn^{2+}$ levels in HCT116 cells, whereas its inactive enantiomer had no effect (Figure 6A). This effect was reproduced using a range of structurally different BETi (OTX015, I-BET762, and I-BET151 [Amorim et al., 2016; Zhao et al., 2013]), both in control medium and 50 μM $MnCl_2$ (Figure 6A), consistent with a specific effect of BET bromodomain inhibition on raising intracellular Mn concentration. In addition, these effects were not an atypical feature of HCT116 cells, as they could be observed in Caco-2 colorectal cancer cells (Figure 6B). Further investigation of $Mn^{2+}$ in the JQ1-sensitive HCT116-**ATP2C1** cells showed that their basal level of Mn in 50 μM $MnCl_2$ was highly elevated compared with HCT116-**WT** and further increased upon JQ1 exposure (Figure 6C), suggesting that Mn is involved in their enhanced JQ1 sensitivity.

Finally, we sought direct evidence that JQ1 was selectively increasing intracellular Mn levels by analyzing HCT116 cell pellets for copper, zinc, iron, and manganese ions. JQ1, but not its inactive enantiomer, significantly increased the amount of cellular manganese, providing independent confirmation of the Fura-2 experiments (Figure 6D). In contrast, Cu and Zn levels were unchanged with JQ1. Although Fe levels also appeared unchanged, we could not draw firm conclusions, as many samples were below the limit of detection. The mechanistic basis for increased intracellular Mn ion levels upon BETi treatment has yet to be identified but does not appear to involve changes in ATP2C1 protein expression after JQ1 treatment (Figure S5).

## DISCUSSION

The two bromodomains of the BET proteins have proved highly tractable targets for drug discovery, leading to the identification of many potent pan (BD1 and BD2) (Filippakopoulos and Knapp, 2014) and bromodomain selective LMW inhibitors (Gilan et al., 2020). Intriguingly, BET inhibitors are suggested to have potential for therapeutic application across a diverse array of disease states (Kulikowski et al., 2020) but to realize their therapeutic potential requires increased understanding of how exposure links to cellular signaling and phenotypic outcomes.

Although we identify known genetic vulnerabilities to BETi, we also find an opposite role for some pathways and additional genes not previously described to modulate BETi sensitivity. These differences likely result from the use of diverse experimental conditions across studies that have variously used acute or chronic BETi exposure and cells with different oncogenic drivers. For example, our use of HCT116 cells with a hyper-activating $Kras^{G13D}$ mutant (Ahmed et al., 2013) may explain why our screen suggests that further activation of ERK by JQ1 renders cells more sensitive to BETi, whereas other studies show BETi resistance mediated by ERK signaling (Ma et al., 2017; Togel et al., 2016). Most importantly, our whole genome screens demonstrate that compound concentration alters the range of genes identified as being synergistic with BETi or antagonistic to BETi effects. One likely reason is that BRD4 is differentially sensitive to displacement by BETi from different chromatin binding sites and most sensitive to BETi displacement from super-enhancers, key regulatory sites that are highly enriched in BRD4. Thus, low BETi concentration yields phenotypic outcomes that are not simply an attenuated version of that induced with high dose BETi (Loven et al., 2013). These BRD4-associated super-enhancers are therapeutically relevant, as they are thought to maintain pathological gene expression in inflammatory diseases and cancer (Delmore et al., 2011; Shin et al., 2019; Xu and Vakoc, 2014). Furthermore, we have shown in human

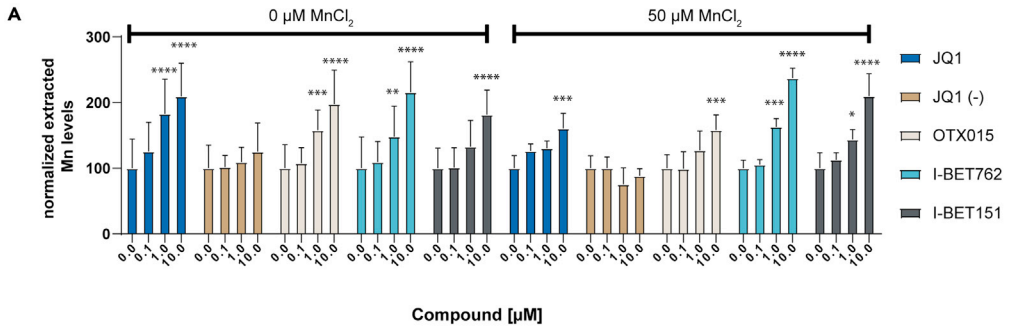


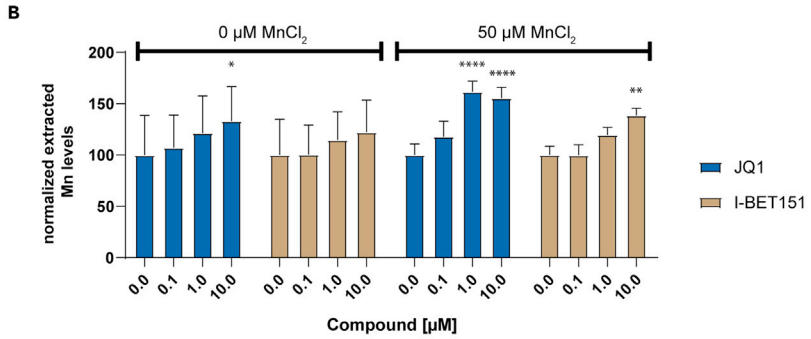


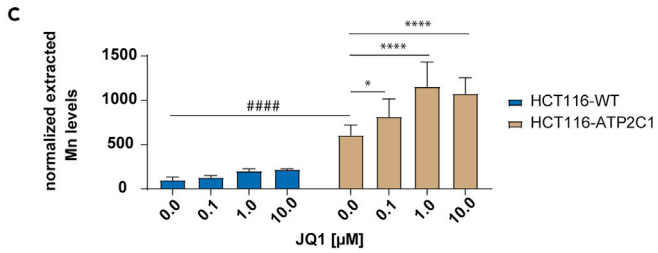


D

Metal Ion Analysis (mg/kg)

| | Cu | | | Fe | | | Mn | | | Zn | | |
|---|---|---|---|---|---|---|---|---|---|---|---|---|
| Untreated | 0.9 | 1 | 1 | <2 | 1.7 | <2 | 1.8 | 2.1 | 2.2 | 14 | 15 | 16 |
| JQ1 | <2 | 0.9 | 0.8 | <10 | <2 | <2 | 4 | 4.7 | 4.6 | 17 | 17 | 16 |
| JQ1 (-) | <2 | 0.9 | 0.8 | <10 | 1.9 | 1.7 | 2.6 | 2.4 | 2.2 | 17 | 16 | 15 |

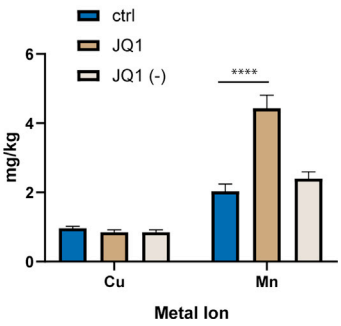


**Figure 6. BET bromodomain inhibitors increase intracellular manganese levels**

(A) Intracellular levels of manganese measured with the Fura-2 assay in HCT116-**WT** cells grown in either control medium or with an additional 50 μM $MnCl_2$. Dose response effects of JQ1, JQ1 (–), the inactive enantiomer of JQ1, OTX015, I-BET762, and I-BET151. Values are normalized to control medium without compound (two-way ANOVA with Dunnett's multiple comparisons test). Mean ± S.D., n = 8. *p = 0.0151, **p = 0.0058, ***p < 0.001, ****p < 0.0001.

(B) Intracellular levels of manganese measured with the Fura-2 assay in Caco-2 cells grown in either control medium or with an additional 50 μM $MnCl_2$. Dose response effects of JQ1 or I-BET151. Values are normalized to control medium without compound (two-way ANOVA with Dunnett's multiple comparisons test) Mean ± S.D., n = 8, *p = 0.0208, **p = 0.0056, ****p < 0.0001.

**Figure 6. *Continued***

(C) Intracellular levels of manganese measured with the Fura-2 assay in HCT116-**WT** compared with HCT116-**ATP2C1** cells in 50 μM $MnCl_2$. Dose response effects of JQ1. Values are normalized to HCT116-**WT** in control medium without compound (two-way ANOVA with Dunnett's multiple comparisons test). Mean ± S.D., n = 8. $^{\#\#\#\#}p < 0.0001$, $^{*}p = 0.0136$, $^{****}p < 0.0001$.

(D) Metal ion analysis using ICP-MS (Inductively Coupled Plasma Mass Spectrometry) was performed on pellets of HCT116-**WT** cells after overnight exposure to either DMSO, 1 μM JQ1, or 1 μM JQ1 (−), the inactive enantiomer (two-way ANOVA with Dunnett's multiple comparisons test). Mean ± S.D., n = 3. $^{****}p < 0.0001$.

keratinocytes that BETi induce exposure-dependent BRD4 chromatin occupancy profiles with some BRD4 occupancy gains, enriched at promoters, observed predominantly at low BETi concentrations (Schutzius et al., 2021). Importantly, a regenerative phenotype is triggered in keratinocytes, *in vitro* and *in vivo*, exclusively by limiting BETi exposure (Schutzius et al., 2021). Likewise, JQ1-induced rescue of function in MeCP2 mutant interneurons (Rett syndrome model) was lost with a too high dosage (Xiang et al., 2020) although the molecular mechanisms responsible were not identified. Interestingly, a recent study identifies the ratio of acylation to acetylation modifications on histones as a regulator of BRD4 chromatin binding affinity with increasing acylation weakening BRD4 binding and enhancing BRD4 mobility (Gao et al., 2021). Mitochondrial function and β-oxidation are important drivers of histone acylation (Gao et al., 2021), and JQ1 increases fatty acid oxidation (Deeney et al., 2016). This raises the possibility that JQ1 regulates BRD4 occupancy directly by displacement and indirectly through changes in histone modifications, leading to greater BRD4 mobility and a pattern of enhanced recruitment at alternative sites dependent upon the level of competition with the compound. Whatever the mechanism, previous findings coupled with our screening data, support exposure-specific effects of BET bromodomain inhibitors. Such effects warrant further investigation to support the clinical use of BET inhibitors by better understanding the essential characteristics and exposure profile of compounds with therapeutic potential in different indications.

Currently the field has focused on the regulation of BETi sensitivity via BRD4 displacement from chromatin (Khoueiry et al., 2019), but the roles of BRD2 and BRD3 are less studied. BET proteins form complex networks on chromatin with histone and nonhistone proteins including each other (Lambert et al., 2018), with JQ1 exerting highly complex effects on individual BET protein interactions and their relative presence in transcriptional complexes (Lambert et al., 2018). Although BET proteins were not resistance hits suggesting some redundancy of function, their role alongside the multiple transcriptional regulators identified in the screen warrants further investigation to dissect the complex transcriptional responses elicited by BETi at different concentrations.

A key discovery from the screen was that ATP2C1 and TMEM165, two functionally linked Golgi-located $Ca^{2+}$/$Mn^{2+}$ transporters that maintain manganese homeostasis, mediate JQ1 resistance. ATP2C1 transports $Mn^{2+}$ into the Golgi lumen and thereby removes excess manganese from the cytosol via the secretory pathway (Horning et al., 2015). TMEM165 also transports manganese from the cytosol to the Golgi (Potelle et al., 2016), and its abundance is directly dependent upon ATP2C1 $Mn^{2+}$ pumping function (Lebredonchel et al., 2019) due to its degradation upon high Mn exposure (Potelle et al., 2017). In Hailey-Hailey patient fibroblasts, with impaired ATP2C1 function, TMEM165 becomes more sensitive to extracellular manganese (Roy et al., 2020). TMEM165 loss is associated with congenital disorders of glycosylation, emphasizing the importance of manganese homeostasis in glycosylation (Foulquier and Legrand, 2020). In this regard, a future avenue for discovery would be to examine protein glycosylation patterns in cells exposed to BETi. We show that extracellular manganese modulates BETi sensitivity, BETi increase cellular Mn, and that editing of ATP2C1 results in higher cellular Mn levels and increased BETi sensitivity. In summary, these findings strongly implicate manganese as a mediator of BETi signaling and argue for Golgi $Mn^{2+}$ efflux rate as a regulator of BETi sensitivity.

Manganese is an essential nutrient and cofactor for many enzymes, playing a key role in multiple fundamental processes such as metabolism and mitochondrial antioxidant systems (Avila et al., 2013). Both Mn deficiency and overexposure are associated with adverse metabolic and neuropsychiatric effects (Balachandran et al., 2020; Li and Yang, 2018), and a recent study highlights the importance of manganese in normal tissue homeostasis (Nakata et al., 2020). $Mn^{2+}$ can directly activate kinases and enhance AKT, ERK, and p38 signaling pathways (Bryan and Bowman, 2017; Peres et al., 2016), but whether Mn mediates the BETi-driven activation of these pathways, suggested by our screen, remains to be determined. Our study strongly implicates manganese as a mediator of BETi signaling, but the mechanism(s) involved and the implications for the clinical use of BETi require further investigation.

In summary, our genome-wide CRISPR screens provide a valuable resource for the development of testable hypotheses to identify novel mediators of the cellular signaling induced by BET bromodomain inhibitors. The value of the screen is demonstrated by the identification of two functionally linked screening hits, ATP2C1 and TMEM165, which led to the discovery that BETi responses involve manganese. Additional interrogation of screening hits has the potential to reveal further mechanistic insights around these and other clinically important proteins such as Tafazzin, which are linked to inherited human diseases. The screen further reveals a diverse set of concentration-dependent genetic mediators of BETi action, which will open avenues for future exploration to understand how exposure might be manipulated to achieve a desired phenotypic outcome. Such studies will seek to identify precise molecular mechanisms of BETi-driven cellular effects, targets for potential combination therapies, and biomarkers to support efficacious exposure and progression of BETi for therapeutic benefit.

### Limitations of the study

Further screens using multiple BETi concentrations, coupled with RNAseq analysis, would provide insights into concentration-dependent responses such as whether they are discrete or continuous.

Additional studies are needed to understand the mechanisms whereby manganese is regulating cell behavior in response to BETi. Further *in vivo* studies, potentially exploring the progression of HCT116 xenografts after exposure to different concentrations of BETi, are needed to evaluate the physiological relevance of our findings.

## STAR★METHODS

Detailed methods are provided in the online version of this paper and include the following:

- KEY RESOURCES TABLE
- RESOURCE AVAILABILITY
  - Lead contact
  - Materials availability
  - Data and code availability
- EXPERIMENTAL MODEL AND SUBJECT DETAILS
  - Cell lines
- METHOD DETAILS
  - Generation of HCT116-Cas9 clone
  - Determination of JQ1 potency
  - sgRNA library design and construction
  - Viral packaging
  - Pooled CRISPR screen in HCT116-Cas9
  - Determination of relative sgRNA abundance
  - Screen data processing and quality analysis
  - Generation of mutant clones and validation
  - JQ1 dose response curves
  - JQ1 dose-response curves in cation solutions
  - Gene expression
  - WES simple western protein analysis
  - FURA-2 method
  - Solvias metal ion analysis
- QUANTIFICATION AND STATISTICAL ANALYSIS

## SUPPLEMENTAL INFORMATION

Supplemental information can be found online at https://doi.org/10.1016/j.isci.2021.103323.

## ACKNOWLEDGMENTS

We thank John Reece-Hoyes and John Alford for their support in the design and generation of the lentiviral libraries; Carsten Russ and Alicia Lindeman for sequencing support; Zinger Yang for data analysis support; and Beat Nyfeler, Julie Bastien, and Felix Lohmann for discussions.

## AUTHOR CONTRIBUTIONS

S.K. and D.H. conceptualized the study, D.E. performed the CRISPR-Cas9 screens, C.K. and F.N. performed the analysis of the CRISPR-Cas9 screens. D.E. G.S., A.M., A.S., and T.W. generated the other data. All authors contributed to data interpretation, generation of figures, and writing the manuscript. All authors reviewed the complete manuscript.

## DECLARATION OF INTERESTS

All authors are employees of Novartis Pharma AG and may own stock in the company.

Received: February 24, 2021
Revised: April 23, 2021
Accepted: October 19, 2021
Published: November 19, 2021

## REFERENCES

Ahmed, D., Eide, P.W., Eilertsen, I.A., Danielsen, S.A., Eknaes, M., Hektoen, M., Lind, G.E., and Lothe, R.A. (2013). Epigenetic and genetic features of 24 colon cancer cell lines. Oncogenesis *2*, e71. https://doi.org/10.1038/oncsis.2013.35.

Ali, I., Conrad, R.J., Verdin, E., and Ott, M. (2018). Lysine acetylation goes global: From epigenetics to metabolism and therapeutics. Chem. Rev. *118*, 1216–1252. https://doi.org/10.1021/acs.chemrev.7b00181.

Alqahtani, A., Choucair, K., Ashraf, M., Hammouda, D.M., Alloghbi, A., Khan, T., Senzer, N., and Nemunaitis, J. (2019). Bromodomain and extra-terminal motif inhibitors: A review of preclinical and clinical advances in cancer therapy. Future Sci. OA *5*, Fso372. https://doi.org/10.4155/fsoa-2018-0115.

Amorim, S., Stathis, A., Gleeson, M., Iyengar, S., Magarotto, V., Leleu, X., Morschhauser, F., Karlin, L., Broussais, F., Rezai, K., et al. (2016). Bromodomain inhibitor OTX015 in patients with lymphoma or multiple myeloma: A dose-escalation, open-label, pharmacokinetic, phase 1 study. Lancet Haematol. *3*, 196–204. https://doi.org/10.1016/s2352-3026(16)00021-1.

Astle, M.V., Hannan, K.M., Ng, P.Y., Lee, R.S., George, A.J., Hsu, A.K., Haupt, Y., Hannan, R.D., and Pearson, R.B. (2012). AKT induces senescence in human cells via mTORC1 and p53 in the absence of DNA damage: Implications for targeting mTOR during malignancy. Oncogene *31*, 1949–1962. https://doi.org/10.1038/onc.2011.394.

Avila, D.S., Puntel, R.L., and Aschner, M. (2013). Manganese in health and disease. Met. Ions Life Sci. *13*, 199–227. https://doi.org/10.1007/978-94-007-7500-8_7.

Balachandran, R.C., Mukhopadhyay, S., McBride, D., Veevers, J., Harrison, F.E., Aschner, M., Haynes, E.N., and Bowman, A.B. (2020). Brain manganese and the balance between essential roles and neurotoxicity. J. Biol. Chem. *295*, 6312–6329. https://doi.org/10.1074/jbc.REV119.009453.

Bechter, O., and Schoffski, P. (2020). Make your best BET: The emerging role of BET inhibitor treatment in malignant tumors. Pharmacol. Ther. *208*, 107479. https://doi.org/10.1016/j.pharmthera.2020.107479.

Bowman, A.B., and Aschner, M. (2014). Considerations on manganese (Mn) treatments for in vitro studies. Neurotoxicology *41*, 141–142. https://doi.org/10.1016/j.neuro.2014.01.010.

Brodsky, R.A. (2009). How I treat paroxysmal nocturnal hemoglobinuria. Blood *113*, 6522–6527. https://doi.org/10.1182/blood-2009-03-195966.

Bryan, M.R., and Bowman, A.B. (2017). Manganese and the insulin-IGF signaling network in Huntington's disease and other neurodegenerative disorders. Adv. Neurobiol. *18*, 113–142. https://doi.org/10.1007/978-3-319-60189-2_6.

Chen, B., Gilbert, L.A., Cimini, B.A., Schnitzbauer, J., Zhang, W., Li, G.W., Park, J., Blackburn, E.H., Weissman, J.S., Qi, L.S., and Huang, B. (2013). Dynamic imaging of genomic loci in living human cells by an optimized CRISPR/Cas system. Cell *155*, 1479–1491. https://doi.org/10.1016/j.cell.2013.12.001.

Cochran, A.G., Conery, A.R., and Sims, R.J., 3rd (2019). Bromodomains: A new target class for drug development. Nat. Rev. Drug Discov. https://doi.org/10.1038/s41573-019-0030-7.

Colinet, A.S., Sengottaiyan, P., Deschamps, A., Colsoul, M.L., Thines, L., Demaegd, D., Duchene, M.C., Foulquier, F., Hols, P., and Morsomme, P. (2016). Yeast Gdt1 is a Golgi-localized calcium transporter required for stress-induced calcium signaling and protein glycosylation. Sci. Rep. *6*, 24282. https://doi.org/10.1038/srep24282.

Core, L., and Adelman, K. (2019). Promoter-proximal pausing of RNA polymerase II: A nexus of gene regulation. Genes Dev. *33*, 960–982. https://doi.org/10.1101/gad.325142.119.

Dai, X., Gan, W., Li, X., Wang, S., Zhang, W., Huang, L., Liu, S., Zhong, Q., Guo, J., Zhang, J., et al. (2017). Prostate cancer-associated SPOP mutations confer resistance to BET inhibitors through stabilization of BRD4. Nat. Med. *23*, 1063–1071. https://doi.org/10.1038/nm.4378.

Deeney, J.T., Belkina, A.C., Shirihai, O.S., Corkey, B.E., and Denis, G.V. (2016). BET bromodomain proteins Brd2, Brd3 and Brd4 selectively regulate metabolic pathways in the pancreatic beta-cell. PLoS One *11*, e0151329. https://doi.org/10.1371/journal.pone.0151329.

DeJesus, R., Moretti, F., McAllister, G., Wang, Z., Bergman, P., Liu, S., Frias, E., Alford, J., Reece-Hoyes, J.S., Lindeman, A., et al. (2016). Functional CRISPR screening identifies the ufmylation pathway as a regulator of SQSTM1/p62. Elife *5*. https://doi.org/10.7554/eLife.17290.

Delmore, J.E., Issa, G.C., Lemieux, M.E., Rahl, P.B., Shi, J., Jacobs, H.M., Kastritis, E., Gilpatrick, T., Paranal, R.M., Qi, J., et al. (2011). BET bromodomain inhibition as a therapeutic strategy to target c-Myc. Cell *146*, 904–917. https://doi.org/10.1016/j.cell.2011.08.017.

Deng, H., and Xiao, H. (2017). The role of the ATP2C1 gene in Hailey-Hailey disease. Cell Mol. Life Sci. *74*, 3687–3696. https://doi.org/10.1007/s00018-017-2544-7.

Donati, B., Lorenzini, E., and Ciarrocchi, A. (2018). BRD4 and cancer: Going beyond transcriptional regulation. Mol. Cancer *17*, 164. https://doi.org/10.1186/s12943-018-0915-9.

Doudna, J.A., and Charpentier, E. (2014). Genome editing. The new frontier of genome engineering with CRISPR-Cas9. Science *346*, 1258096. https://doi.org/10.1126/science.1258096.

Duan, Q., McMahon, S., Anand, P., Shah, H., Thomas, S., Salunga, H.T., Huang, Y., Zhang, R., Sahadevan, A., Lemieux, M.E., et al. (2017). BET bromodomain inhibition suppresses innate inflammatory and profibrotic transcriptional networks in heart failure. Sci. Transl. Med. *9*. https://doi.org/10.1126/scitranslmed.aah5084.

Estoppey, D., Hewett, J.W., Guy, C.T., Harrington, E., Thomas, J.R., Schirle, M., Cuttat, R., Waldt, A., Gerrits, B., Yang, Z., et al. (2017). Identification of a novel NAMPT inhibitor by CRISPR/Cas9 chemogenomic profiling in mammalian cells. Sci. Rep. *7*, 42728. https://doi.org/10.1038/srep42728.

Fang, L., El Wazan, L., Tan, C., Nguyen, T., Hung, S.S.C., Hewitt, A.W., and Wong, R.C.B. (2018). Potentials of cellular reprogramming as a novel strategy for neuroregeneration. Front. Cell. Neurosci. *12*, 460. https://doi.org/10.3389/fncel.2018.00460.

Filippakopoulos, P., and Knapp, S. (2014). Targeting bromodomains: Epigenetic readers of lysine acetylation. Nat. Rev. Drug Discov. *13*, 337–356. https://doi.org/10.1038/nrd4286.

Filippakopoulos, P., Qi, J., Picaud, S., Shen, Y., Smith, W.B., Fedorov, O., Morse, E.M., Keates, T., Hickman, T.T., Felletar, I., et al. (2010). Selective inhibition of BET bromodomains. Nature *468*, 1067–1073. https://doi.org/10.1038/nature09504.

Foulquier, F., and Legrand, D. (2020). Biometals and glycosylation in humans: Congenital disorders of glycosylation shed lights into the crucial role of Golgi manganese homeostasis. Biochim. Biophys. Acta Gen. Subj. *1864*, 129674. https://doi.org/10.1016/j.bbagen.2020.129674.

French, C.A. (2016). Small-molecule targeting of BET proteins in cancer. Adv. Cancer Res. *131*, 21–58. https://doi.org/10.1016/bs.acr.2016.04.001.

Gao, M., Wang, J., Rousseaux, S., Tan, M., Pan, L., Peng, L., Wang, S., Xu, W., Ren, J., Liu, Y., et al. (2021). Metabolically controlled histone H4K5 acylation/acetylation ratio drives BRD4 genomic distribution. Cell Rep. *36*, 109460. https://doi.org/10.1016/j.celrep.2021.109460.

Gilan, O., Rioja, I., Knezevic, K., Bell, M.J., Yeung, M.M., Harker, N.R., Lam, E.Y.N., Chung, C.W., Bamborough, P., Petretich, M., et al. (2020). Selective targeting of BD1 and BD2 of the BET proteins in cancer and immunoinflammation. Science *368*, 387–394. https://doi.org/10.1126/science.aaz8455.

Guo, L., Cui, C., Zhang, K., Wang, J., Wang, Y., Lu, Y., Chen, K., Yuan, J., Xiao, G., Tang, B., et al. (2019). Kindlin-2 links mechano-environment to proline synthesis and tumor growth. Nat. Commun. *10*, 845. https://doi.org/10.1038/s41467-019-08772-3.

Hajmirza, A., Emadali, A., Gauthier, A., Casasnovas, O., Gressin, R., and Callanan, M.B. (2018). BET family protein BRD4: An emerging actor in NFkappaB signaling in inflammation and cancer. Biomedicines *6*. https://doi.org/10.3390/biomedicines6010016.

Helmlinger, D., and Tora, L. (2017). Sharing the SAGA. Trends Biochem. Sci. *42*, 850–861. https://doi.org/10.1016/j.tibs.2017.09.001.

Hoepfner, D., McAllister, G., and Hoffman, G.R. (2019). CRISPR/Cas9-based chemogenomic profiling in mammalian cells. Methods Mol. Biol. *1888*, 153–174. https://doi.org/10.1007/978-1-4939-8891-4_9.

Hoffman, G.R., Rahal, R., Buxton, F., Xiang, K., McAllister, G., Frias, E., Bagdasarian, L., Huber, J., Lindeman, A., Chen, D., et al. (2014). Functional epigenetics approach identifies BRM/SMARCA2 as a critical synthetic lethal target in BRG1-deficient cancers. Proc. Natl. Acad. Sci. U S A *111*, 3128–3133. https://doi.org/10.1073/pnas.1316793111.

Horning, K.J., Caito, S.W., Tipps, K.G., Bowman, A.B., and Aschner, M. (2015). Manganese is essential for neuronal health. Annu. Rev. Nutr. *35*, 71–108. https://doi.org/10.1146/annurev-nutr-071714-034419.

Jahagirdar, R., Attwell, S., Marusic, S., Bendele, A., Shenoy, N., McLure, K.G., Gilham, D., Norek, K., Hansen, H.C., Yu, R., et al. (2017). RVX-297, a BET bromodomain inhibitor, has therapeutic effects in preclinical models of acute inflammation and autoimmune disease. Mol. Pharmacol. *92*, 694–706. https://doi.org/10.1124/mol.117.110379.

Khoueiry, P., Ward Gahlawat, A., Petretich, M., Michon, A.M., Simola, D., Lam, E., Furlong, E.E., Benes, V., Dawson, M.A., Prinjha, R.K., et al. (2019). BRD4 bimodal binding at promoters and drug-induced displacement at Pol II pause sites associates with I-BET sensitivity. Epigenetics Chromatin *12*, 39. https://doi.org/10.1186/s13072-019-0286-5.

Kidger, A.M., Rushworth, L.K., Stellzig, J., Davidson, J., Bryant, C.J., Bayley, C., Caddye, E., Rogers, T., Keyse, S.M., and Caunt, C.J. (2017). Dual-specificity phosphatase 5 controls the localized inhibition, propagation, and transforming potential of ERK signaling. Proc. Natl. Acad. Sci. U S A *114*, 317–326. https://doi.org/10.1073/pnas.1614684114.

Knutson, B.A., Smith, M.L., Walker-Kopp, N., and Xu, X. (2016). Super elongation complex contains a TFIIF-related subcomplex. Transcription *7*, 133–140. https://doi.org/10.1080/21541264.2016.1194027.

Konig, R., Chiang, C.Y., Tu, B.P., Yan, S.F., DeJesus, P.D., Romero, A., Bergauer, T., Orth, A., Krueger, U., Zhou, Y., and Chanda, S.K. (2007). A probability-based approach for the analysis of large-scale RNAi screens. Nat. Methods *4*, 847–849. https://doi.org/10.1038/nmeth1089.

Kulikowski, E., Rakai, B.D., and Wong, N.C.W. (2020). Inhibitors of bromodomain and extra-terminal proteins for treating multiple human diseases. Med. Res. Rev. https://doi.org/10.1002/med.21730.

Kumar, K.K., Lowe, E.W., Jr., Aboud, A.A., Neely, M.D., Redha, R., Bauer, J.A., Odak, M., Weaver, C.D., Meiler, J., Aschner, M., and Bowman, A.B. (2014). Cellular manganese content is developmentally regulated in human dopaminergic neurons. Sci. Rep. *4*, 6801. https://doi.org/10.1038/srep06801.

Kwakye, G.F., Li, D., and Bowman, A.B. (2011). Novel high-throughput assay to assess cellular manganese levels in a striatal cell line model of Huntington's disease confirms a deficit in manganese accumulation. Neurotoxicology *32*, 630–639. https://doi.org/10.1016/j.neuro.2011.01.002.

Lambert, J.P., Picaud, S., Fujisawa, T., Hou, H., Savitsky, P., Uuskula-Reimand, L., Gupta, G.D., Abdouni, H., Lin, Z.Y., Tucholska, M., et al. (2018). Interactome rewiring following pharmacological targeting of BET bromodomains. Mol. Cell. https://doi.org/10.1016/j.molcel.2018.11.006.

Langmead, B., Trapnell, C., Pop, M., and Salzberg, S.L. (2009). Ultrafast and memory-efficient alignment of short DNA sequences to the human genome. Genome Biol. *10*, R25. https://doi.org/10.1186/gb-2009-10-3-r25.

Lebredonchel, E., Houdou, M., Hoffmann, H.H., Kondratska, K., Krzewinski, M.A., Vicogne, D., Rice, C.M., Klein, A., and Foulquier, F. (2019). Investigating the functional link between TMEM165 and SPCA1. Biochem. J. *476*, 3281–3293. https://doi.org/10.1042/BCJ20190488.

Leung, G.P., Feng, T., Sigoillot, F.D., Geyer, F.C., Shirley, M.D., Ruddy, D.A., Rakiec, D.P., Freeman, A.K., Engelman, J.A., Jaskelioff, M., and Stuart, D.D. (2019). Hyperactivation of MAPK signaling is deleterious to RAS/RAF-mutant melanoma. Mol. Cancer Res. *17*, 199–211. https://doi.org/10.1158/1541-7786.MCR-18-0327.

Li, L., and Yang, X. (2018). The essential element manganese, oxidative stress, and metabolic diseases: Links and interactions. Oxid. Med. Cell Longev. *2018*, 7580707. https://doi.org/10.1155/2018/7580707.

Lin, S., and Du, L. (2020). The therapeutic potential of BRD4 in cardiovascular disease. Hypertens. Res. *43*, 1006–1014. https://doi.org/10.1038/s41440-020-0459-4.

Love, M.I., Huber, W., and Anders, S. (2014). Moderated estimation of fold change and dispersion for RNA-seq data with DESeq2. Genome Biol. *15*, 550. https://doi.org/10.1186/s13059-014-0550-8.

Loven, J., Hoke, H.A., Lin, C.Y., Lau, A., Orlando, D.A., Vakoc, C.R., Bradner, J.E., Lee, T.I., and Young, R.A. (2013). Selective inhibition of tumor oncogenes by disruption of super-enhancers. Cell *153*, 320–334. https://doi.org/10.1016/j.cell.2013.03.036.

Lynch, C.J., Bernad, R., Calvo, I., Nobrega-Pereira, S., Ruiz, S., Ibarz, N., Martinez-Val, A., Grana-Castro, O., Gomez-Lopez, G., Andres-Leon, E., et al. (2018). The RNA polymerase II factor RPAP1 is critical for mediator-driven transcription and cell identity. Cell Rep. *22*, 396–410. https://doi.org/10.1016/j.celrep.2017.12.062.

Lynch, C.J., Bernad, R., Martinez-Val, A., Shahbazi, M.N., Nobrega-Pereira, S., Calvo, I., Blanco-Aparicio, C., Tarantino, C., Garreta, E., Richart-Gines, L., et al. (2020). Global hyperactivation of enhancers stabilizes human and mouse naive pluripotency through inhibition of CDK8/19 mediator kinases. Nat. Cell Biol. *22*, 1223–1238. https://doi.org/10.1038/s41556-020-0573-1.

Ma, Y., Wang, L., Neitzel, L.R., Loganathan, S.N., Tang, N., Qin, L., Crispi, E.E., Guo, Y., Knapp, S., Beauchamp, R.D., et al. (2017). The MAPK pathway regulates intrinsic resistance to BET inhibitors in colorectal cancer. Clin. Cancer Res. *23*, 2027–2037. https://doi.org/10.1158/1078-0432.ccr-16-0453.

Marcotte, R., Sayad, A., Brown, K.R., Sanchez-Garcia, F., Reimand, J., Haider, M., Virtanen, C., Bradner, J.E., Bader, G.D., Mills, G.B., et al. (2016). Functional genomic landscape of human breast cancer drivers, vulnerabilities, and resistance. Cell *164*, 293–309. https://doi.org/10.1016/j.cell.2015.11.062.

Menzl, I., Witalisz-Siepracka, A., and Sexl, V. (2019). CDK8-novel therapeutic opportunities. Pharmaceuticals *12*. https://doi.org/10.3390/ph12020092.

Middleton, S.A., Rajpal, N., Cutler, L., Mander, P., Rioja, I., Prinjha, R.K., Rajpal, D., Agarwal, P., and Kumar, V. (2018). BET inhibition improves NASH and liver fibrosis. Sci. Rep. *8*, 17257. https://doi.org/10.1038/s41598-018-35653-4.

Nakata, T., Creasey, E.A., Kadoki, M., Lin, H., Selig, M.K., Yao, J., Lefkovith, A., Daly, M.J., Graham, D.B., and Xavier, R.J. (2020). A missense variant in SLC39A8 confers risk for Crohn's disease by disrupting manganese homeostasis and intestinal barrier integrity. Proc. Natl. Acad. Sci. U S A *117*, 28930–28938. https://doi.org/10.1073/pnas.2014742117.

Peres, T.V., Schettinger, M.R., Chen, P., Carvalho, F., Avila, D.S., Bowman, A.B., and Aschner, M. (2016). Manganese-induced neurotoxicity: A review of its behavioral consequences and neuroprotective strategies. BMC Pharmacol. Toxicol. *17*, 57. https://doi.org/10.1186/s40360-016-0099-0.

Piha-Paul, S.A., Sachdev, J.C., Barve, M., LoRusso, P., Szmulewitz, R., Patel, S.P., Lara, P.N., Jr., Chen, X., Hu, B., Freise, K.J., et al. (2019). First-in-Human study of Mivebresib (ABBV-075), an oral pan-inhibitor of bromodomain and extra terminal proteins, in patients with relapsed/refractory solid tumors. Clin. Cancer Res. https://doi.org/10.1158/1078-0432.ccr-19-0578.

Potelle, S., Dulary, E., Climer, L., Duvet, S., Morelle, W., Vicogne, D., Lebredonchel, E., Houdou, M., Spriet, C., Krzewinski-Recchi, M.A., et al. (2017). Manganese-induced turnover of TMEM165. Biochem. J. *474*, 1481–1493. https://doi.org/10.1042/bcj20160910.

Potelle, S., Morelle, W., Dulary, E., Duvet, S., Vicogne, D., Spriet, C., Krzewinski-Recchi, M.A., Morsomme, P., Jaeken, J., Matthijs, G., et al. (2016). Glycosylation abnormalities in Gdt1p/TMEM165 deficient cells result from a defect in Golgi manganese homeostasis. Hum. Mol. Genet. *25*, 1489–1500. https://doi.org/10.1093/hmg/ddw026.

Potting, C., Crochemore, C., Moretti, F., Nigsch, F., Schmidt, I., Manneville, C., Carbone, W., Knehr, J., DeJesus, R., Lindeman, A., et al. (2018). Genome-wide CRISPR screen for PARKIN regulators reveals transcriptional repression as a determinant of mitophagy. Proc. Natl. Acad. Sci. U S A *115*, 180–189. https://doi.org/10.1073/pnas.1711023115.

Roy, A.S., Miskinyte, S., Garat, A., Hovnanian, A., Krzewinski-Recchi, M.A., and Foulquier, F. (2020). SPCA1 governs the stability of TMEM165 in Hailey-Hailey disease. Biochimie *174*, 159–170. https://doi.org/10.1016/j.biochi.2020.04.017.

Sancak, Y., Bar-Peled, L., Zoncu, R., Markhard, A.L., Nada, S., and Sabatini, D.M. (2010). Ragulator-Rag complex targets mTORC1 to the lysosomal surface and is necessary for its activation by amino acids. Cell *141*, 290–303. https://doi.org/10.1016/j.cell.2010.02.024.

Schutzius, G., Kolter, C., Bergling, S., Tortelli, F., Fuchs, F., Renner, S., Guagnano, V., Cotesta, S., Rueeger, H., Faller, M., et al. (2021). BET bromodomain inhibitors regulate keratinocyte plasticity. Nat. Chem. Biol. https://doi.org/10.1038/s41589-020-00716-z.

Shalem, O., Sanjana, N.E., Hartenian, E., Shi, X., Scott, D.A., Mikkelson, T., Heckl, D., Ebert, B.L., Root, D.E., Doench, J.G., and Zhang, F. (2014). Genome-scale CRISPR-Cas9 knockout screening in human cells. Science *343*, 84–87. https://doi.org/10.1126/science.1247005.

Shi, J., and Vakoc, C.R. (2014). The mechanisms behind the therapeutic activity of BET bromodomain inhibition. Mol. Cell *54*, 728–736. https://doi.org/10.1016/j.molcel.2014.05.016.

Shin, J.Y., Beckett, J.D., Bagirzadeh, R., Creamer, T.J., Shah, A.A., McMahan, Z., Paik, J.J., Sampedro, M.M., MacFarlane, E.G., Beer, M.A., et al. (2019). Epigenetic activation and memory at a TGFB2 enhancer in systemic sclerosis. Sci. Transl. Med. *11*. https://doi.org/10.1126/scitranslmed.aaw0790.

Shu, S., Wu, H.J., Ge, J.Y., Zeid, R., Harris, I.S., Jovanovic, B., Murphy, K., Wang, B., Qiu, X., Endress, J.E., et al. (2020). Synthetic lethal and resistance interactions with BET bromodomain inhibitors in triple-negative breast cancer. Mol. Cell *78*, 1096–1113.e8. https://doi.org/10.1016/j.molcel.2020.04.027.

Sossey-Alaoui, K., Pluskota, E., Szpak, D., and Plow, E.F. (2019). The Kindlin2-p53-SerpinB2 signaling axis is required for cellular senescence in breast cancer. Cell Death Dis. *10*, 539. https://doi.org/10.1038/s41419-019-1774-z.

Togel, L., Nightingale, R., Chueh, A.C., Jayachandran, A., Tran, H., Phesse, T., Wu, R., Sieber, O.M., Arango, D., Dhillon, A.S., et al. (2016). Dual targeting of bromodomain and extraterminal domain proteins, and WNT or MAPK signaling, inhibits c-MYC expression and proliferation of colorectal cancer cells. Mol. Cancer Ther. *15*, 1217–1226. https://doi.org/10.1158/1535-7163.mct-15-0724.

Tsimberidou, A.M., Letourneau, K., Fu, S., Hong, D., Naing, A., Wheler, J., Uehara, C., McRae, S.E., Wen, S., and Kurzrock, R. (2011). Phase I clinical trial of hepatic arterial infusion of paclitaxel in patients with advanced cancer and dominant liver involvement. Cancer Chemother. Pharmacol. *68*, 247–253. https://doi.org/10.1007/s00280-010-1482-y.

Wang, S., Zhang, S., Zhao, Z., Zhang, C., Yang, X., and Wang, Y. (2017). Connexin 43 enhances paclitaxel cytotoxicity in colorectal cancer cell lines. Exp. Ther. Med. *14*, 1212–1218. https://doi.org/10.3892/etm.2017.4589.

Wang, T., Wei, J.J., Sabatini, D.M., and Lander, E.S. (2014). Genetic screens in human cells using the CRISPR-Cas9 system. Science *343*, 80–84. https://doi.org/10.1126/science.1246981.

Wang, X., De Geyter, C., Jia, Z., Peng, Y., and Zhang, H. (2020). HECTD1 regulates the expression of SNAIL: Implications for epithelial mesenchymal transition. Int. J. Oncol. *56*, 1186–1198. https://doi.org/10.3892/ijo.2020.5002.

Wasmus, C., and Dudek, J. (2020). Metabolic alterations caused by defective cardiolipin remodeling in inherited cardiomyopathies. Life (Basel) *10*. https://doi.org/10.3390/life10110277.

Xia, Z., Wei, J., Li, Y., Wang, J., Li, W., Wang, K., Hong, X., Zhao, L., Chen, C., Min, J., and Wang, F. (2017). Zebrafish slc30a10 deficiency revealed a novel compensatory mechanism of Atp2c1 in maintaining manganese homeostasis. PLoS Genet. *13*, e1006892. https://doi.org/10.1371/journal.pgen.1006892.

Xiang, Y., Tanaka, Y., Patterson, B., Hwang, S.M., Hysolli, E., Cakir, B., Kim, K.Y., Wang, W., Kang, Y.J., Clement, E.M., et al. (2020). Dysregulation of BRD4 function underlies the functional abnormalities of MeCP2 mutant neurons. Mol. Cell *79*, 84–98.e9. https://doi.org/10.1016/j.molcel.2020.05.016.

Xu, Y., Bernecky, C., Lee, C.T., Maier, K.C., Schwalb, B., Tegunov, D., Plitzko, J.M., Urlaub, H., and Cramer, P. (2017). Architecture of the RNA polymerase II-Paf1C-TFIIS transcription elongation complex. Nat. Commun. *8*, 15741. https://doi.org/10.1038/ncomms15741.

Xu, Y., Li, N., Xiang, R., and Sun, P. (2014). Emerging roles of the p38 MAPK and PI3K/AKT/mTOR pathways in oncogene-induced senescence. Trends Biochem. Sci. *39*, 268–276. https://doi.org/10.1016/j.tibs.2014.04.004.

Xu, Y., and Vakoc, C.R. (2014). Brd4 is on the move during inflammation. Trends Cell Biol. *24*, 615–616. https://doi.org/10.1016/j.tcb.2014.09.005.

Zatreanu, D., Han, Z., Mitter, R., Tumini, E., Williams, H., Gregersen, L., Dirac-Svejstrup, A.B., Roma, S., Stewart, A., Aguilera, A., and Svejstrup, J.Q. (2019). Elongation factor TFIIS prevents transcription stress and R-loop accumulation to maintain genome stability. Mol. Cell. https://doi.org/10.1016/j.molcel.2019.07.037.

Zhang, J., Dulak, A.M., Hattersley, M.M., Willis, B.S., Nikkila, J., Wang, A., Lau, A., Reimer, C., Zinda, M., Fawell, S.E., et al. (2018). BRD4 facilitates replication stress-induced DNA damage response. Oncogene *37*, 3763–3777. https://doi.org/10.1038/s41388-018-0194-3.

Zhao, Y., Liu, J., Chen, F., and Feng, X.H. (2018). C-terminal domain small phosphatase-like 2 promotes epithelial-to-mesenchymal transition via Snail dephosphorylation and stabilization. Open Biol. *8*. https://doi.org/10.1098/rsob.170274.

Zhao, Y., Yang, C.Y., and Wang, S. (2013). The making of I-BET762, a BET bromodomain inhibitor now in clinical development. J. Med. Chem. *56*, 7498–7500. https://doi.org/10.1021/jm4014407.

## STAR★METHODS

### KEY RESOURCES TABLE

| REAGENT or RESOURCE | SOURCE | IDENTIFIER |
|---|---|---|
| **Antibodies** | | |
| Rabbit polyclonal anti-ATP2C1 | Invitrogen | Cat#PA5-109430 |
| **Chemicals, peptides, and recombinant proteins** | | |
| JQ1 | Selleckchem | Cat#S7110 |
| JQ1 (-) | Outsourced at Pharmaron | N/A |
| OTX015 | Cayman Chemicals | Cat#15947 |
| I-BET151 | Synthesized in house | N/A |
| I-BET762 | Outsourced at WuXi | N/A |
| Paclitaxel | Sigma | Cat#T7402 |
| FLAER | Cedarlanelabs | Cat#FL2S |
| Fura-2 (ultra-pure) | Enzo Life Sciences | Cat#ENZ-52007 |
| $CaCl_2$ | Sigma | Cat#21097 |
| $MnCl_2$ | Sigma | Cat#M1787 |
| **Critical commercial assays** | | |
| CellTiter-Glo Luminescent Cell Viability Assay | Promega | Cat#G7573 |
| Quant-iT Pico Green dsDNA Assay Kit | Thermo Fisher Scientific | Cat#P11496 |
| Pierce™ BCA Protein Assay Kit | Thermo Fisher Scientific | Cat#23225 |
| EZ Standard Pack 1 for WES | Protein Simple | Cat#PS-ST01EZ-8 |
| KAPA SYBR Fast Once-step Universal qPCR Kit | Kapa | Cat#KK4652 |
| Purelink Genomic DNA Mini Kit | Thermo Fisher Scientific | Cat#K182002 |
| QIAamp DNA blood maxi kit | Qiagen | Cat#51194 |
| QIAamp DNA mini Kit | Qiagen | Cat#51304 |
| RNeasy® Plus Mini kit | Qiagen | Cat#74134 |
| Zymoclean Gel DNA Recovery Kit | Zymo Research | Cat#D4001 |
| **Deposited data** | | |
| CRISPR public data | https://doi.org/10.1016/j.molcel.2020.04.027 | N/A |
| CRISPR data | Tables S1, S2, S3, S4, S5, S6, S7, S8, S9, S10, and S11 | N/A |
| **Experimental models: Cell lines** | | |
| HCT116 | ATCC | RRID: CVCL_0291 |
| HCT116-Cas9 | Estoppey et al., 2017 (https://doi.org/10.1038/srep42728) | N/A |
| HCT116-ATP2C1 | This paper | N/A |
| HCT116-FERMT2 | This paper | N/A |
| HCT116-DUSP5 | This paper | N/A |
| Caco-2 | ATCC | RRID: CVCL_0025 |
| HT-29 | ATCC | RRID: CVCL_0320 |
| SUM159PT | Asterand Biosciences | RRID: CVCL_5423 |
| **Oligonucleotides** | | |
| sgRNA sequence targeting ATP2C1 : GAACTCTATCCCCAACAGAA | This paper | N/A |

(*Continued on next page*)

*Continued*

| REAGENT or RESOURCE | SOURCE | IDENTIFIER |
|---|---|---|
| sgRNA sequence targeting FERMT2 : GGTGGGAAAAGAAGAGAACT | This paper | N/A |
| sgRNA sequence targeting DUSP5 : GCGCTACGTGCTGCCCGACG | This paper | N/A |
| sgRNA sequence targeting PIGA : TGGCGTGGAAGAGAGCATCA | This paper | N/A |
| qPCR Primer: RPL32RT Forward: AAACCCAGAGGCATTGACAAC | This paper | N/A |
| qPCR Primer: RPL32RT Reverse: TAACCAATGTTGGGCATCAAG | This paper | N/A |
| qPCR Primer: ATP2C1 Forward: GCCGTGGCTGACACTAAAGAC | This paper | N/A |
| qPCR Primer: ATP2C1 Reverse: TTTTGAAAACGTGCAACCTTCATTT | This paper | N/A |
| Recombinant DNA | | |
| pLenti6 | Invitrogen | Cat#V49610 |
| pNGx-LV-g003 | DeJesus et al., 2016 (https://doi.org/10.7554/eLife.17290) | N/A |
| Software and algorithms | | |
| R | http://www.R-project.org/ | N/A |
| bcl2fastq2 (version 2.17.1.14) | http://support.illumina.com/downloads/bcl2fastq-conversion-software-v217.html | N/A |
| fastx-toolkit (version 0.0.13) | http://hannonlab.cshl.edu/fastx_toolkit/index.html | N/A |
| Bowtie | Langmead et al., 2009 (https://doi.org/10.1186/gb-2009-10-3-r25) | N/A |
| RSA | Konig et al., 2007 (https://doi.org/10.1038/nmeth1089) and Potting et al., 2018 (https://doi.org/10.1073/pnas.1711023115) | N/A |
| Gene set analysis | In-house tool using a hypergeometric test | N/A |
| DESeq2 | Love et al., 2014 (https://doi.org/10.1186/s13059-014-0550-8) | N/A |
| GraphPad Prism version 9.1.2 | GraphPad Software, Inc | https://www.graphpad.com/scientific-software/prism/ |
| Tibco Spotfire version 6.5.3 | Tibco Software, Inc | https://www.tibco.com/ |

## RESOURCE AVAILABILITY

### Lead contact

Further information and requests for resources and reagents should be directed to and will be fulfilled by the lead contact, Dominic Hoepfner (Dominic.Hoepfner@novartis.com).

### Materials availability

NIBR is committed to support scientific research and cell lines generated in this article can be provided under MTA.

### Data and code availability

- CRISPR screening data and key results are provided in the Tables S1, S2, S3, S4, S5, S6, S7, S8, S9, S10, and S11. This paper also analyzes existing, publicly available data. DOIs for the datasets are listed in the

key resources table. All additional data reported in this paper will be shared by the lead contact upon request.

- All original code has been published. DOIs are listed in the key resources table.
- Any additional information required to reanalyze the data reported in this paper is available from the lead contact upon request.

## EXPERIMENTAL MODEL AND SUBJECT DETAILS

### Cell lines

*HCT116 cells (RRID: CVCL_0291).* *Origin*: Human colon carcinoma cell line obtained from a 48-year-old male

*Culture and media conditions:* HCT116 cells were obtained from ATCC (#CCL-247) and grown in DMEM high glucose, Glutamax, pyruvate (Thermo Fisher Scientific, 31966021) supplemented with 10% FBS and 5%Pen/strep. Cells were maintained in a 37°C incubator under 5% $CO_2$. We did not authenticate this cell line in our laboratory.

*Caco-2 cells (RRID: CVCL_0025).* *Origin:* Human colon adenocarcinoma cell line obtained from a 72-year-old male

*Culture and media conditions:* Caco-2 cells were obtained from ATCC (#HTB-37) and grown in DMEM high glucose, Glutamax, pyruvate (Thermo Fisher Scientific, 31966021) supplemented with 10% FBS and 5%Pen/strep. Cells were maintained in a 37°C incubator under 5% $CO_2$. We did not authenticate this cell line in our laboratory.

*HT-29 cells (RRID: CVCL_0320).* *Origin:* Human colon adenocarcinoma cell line obtained from a 44-year-old female

*Culture and media conditions:* HT-29 cells were obtained from ATCC (#HTB-38) and grown in DMEM high glucose, Glutamax, pyruvate (Thermo Fisher Scientific, 31966021) supplemented with 10% FBS and 5%Pen/strep. Cells were maintained in a 37°C incubator under 5% $CO_2$. We did not authenticate this cell line in our laboratory.

*SUM159PT cells (RRID: CVCL_5423).* *Origin:* Human breast pleomorphic carcinoma cell line obtained from a 71-year-old female

*Culture and media conditions:* SUM159PT cells were obtained from Asterand Biosciences and grown in DMEM high glucose, Glutamax, pyruvate (Thermo Fisher Scientific, 31966021) supplemented with 10% FBS and 5% Pen/strep. Cells were maintained in a 37°C incubator under 5% $CO_2$. We did not authenticate this cell line in our laboratory.

## METHOD DETAILS

### Generation of HCT116-Cas9 clone

The Cas9 gene encoding the *S. pyogenes* CRISPR associated protein 9 RNA-guided DNA endonuclease Cas9 (Doudna and Charpentier, 2014) was cloned under control of the human cytomegalovirus (CMV) promoter into a lentiviral construct derived from pLenti6 (#V49610, Invitrogen) carrying a blasticidin resistance cassette. Upon packaging, the active virus was used to transduce the construct into HCT116 cells (#CCL-247, ATCC) grown in DMEM high glucose (#31966047, Life Technologies). Blasticidin-resistant clones were picked, analyzed for Cas9 expression and assessed for editing using a short guide RNA (sgRNA) against PIG-A encoding an enzyme in the glycophosphatidylinositol (GPI) anchor biosynthesis pathway with the following sequence: 5'-TGGCGTGGAAGAGAGCATCA-3' by a genetic adaptation of the FLAER (Fluorescently, Alexa488-labeled, inactive variant of aerolysin) assay (Brodsky, 2009). Cells were infected with the PIG-A sgRNA and a control at a multiplicity of infection (M.O.I.) of 1, then selected with puromycin (2 μg/ml) for 4 days. Transduction efficiency was assessed by flow cytometry using the red fluorescent protein (RFP) reporter encoded on the lentiviral construct. If >90% RFP positive cells were measured selective pressure was removed and the cells grown without puromycin. Decrease of GPI anchored proteins from the

cell surface as an indirect measure of PIG-A editing/inactivation was measured by staining both control and PIG-A infected cells with the FLAER reagent (#FL2S, Cedarlanelabs) as follows: 100'000 cells/well in a fluorescence-activated cell sorting (FACS) compatible microwell plate were washed twice with PBS, and after removal of the supernatant 100 µl/well FLAER master mix added (1:100 diluted FL2S stock in 3% BSA) the cells gently resuspended and incubated in the dark at 37°C/5% CO2 for 20 minutes. Then cells were washed twice in phosphate buffered saline (PBS), resuspended and analyzed by flow cytometry for percentage of stained/unstained cells. Control cells were used to set correct gating parameters. Decreasing levels of stained cells over time indicate functional editing enabling the characterization of the kinetics of editing in the Cas9 positive cell line. Described in detail in (Hoepfner et al., 2019).

### Determination of JQ1 potency

JQ1 was dissolved in dry DMSO (dimethyl sulfoxide) and stored in aliquots at -20°C. A fresh aliquot was thawed for each experiment and the surplus discarded. To enable choice of doses of JQ1 for the pooled CRISPR-Cas9 screen, we analyzed cell proliferation of the HCT116-Cas9 cells. Cells were seeded in 384 well plates, 750 cells/well, in the presence of JQ1 in a dose range between 0.37 nM to 20 µM. The compound solvent (DMSO) was normalized to 0.2 %. 96 hours after compound addition, cell viability was measured using the CellTiter-Glo assay according to the manufacturer's instructions (#G7573, Promega). Data was analyzed and IC50 calculated using the logistic regression curve fit analysis of the Tibco Spotfire package (version 6.5.3, TIBCO Software Inc.). We repeated testing in six well plates, seeding 50'000 HCT116 cells/well testing a narrow dose range (0, 0.05, 0.2, 1 and 10 µM) as directed by the 384 well experiment. 96 hours after compound addition viability was assessed using a Vi-cell XR Cell Viability Analyzer (Beckman Coulter) and curves plotted as described above. The $IC_{20}$ (0.2 µM) and $IC_{50}$ (1 µM) concentrations obtained were used for the screen.

### sgRNA library design and construction

The genome-wide sgRNA library targeting 18,360 protein-coding genes was constructed using chip-based oligonucleotide synthesis to generate spacer-tracrRNA-encoding fragments that were PCR-amplified and cloned as a pool into the BpiI site of the pRSI16 lentiviral plasmid (Cellecta). The modified tracrRNA scaffold (Chen et al., 2013) was used. Olfactory receptors were omitted from the library. The sgRNA designs were based on published sequences (Wang et al., 2014) and five sgRNAs were selected per gene targeting the most proximal 5' exons. 277 genes did not have published sgRNA sequence information and new sgRNAs were designed for these targets that contained an NGG PAM motif, filtering for GC content greater than 40% and less than 80%, eliminating homopolymer stretches greater then 4, and removing any guides with off-target locations having fewer than 4 mismatches across the genome. Sequencing of the plasmid pool showed robust normalization with >90% clones present at a representation of +/- 5-fold from the median counts in the pool. Previous CRISPR/Cas9 screens performed under similar conditions have been previously described in detail (Estoppey et al., 2017; Hoepfner et al., 2019)

The minipool was constructed in a similar way and cloned into the BbsI site of pNGx-LV-g003 lentiviral plasmid (DeJesus et al., 2016). It contained 2698 sgRNA sequences selected for 547 genes. The selected genes included those identified in the whole genome screen as modulating sensitivity or resistance to JQ1, essential genes and a variety of control genes.

### Viral packaging

sgRNA libraries were packaged into lentiviral particles using HEK293T cells as described previously (Hoffman et al., 2014).Packaging was scaled up by growing cells in CellSTACK flasks (#3313, Corning). For each cell stack, 2.1 $e10^7$ cells were transfected 24h after plating using 510.3 µl of TransIT reagent (#MIR2300, Mirus) diluted in 18.4 ml of OPTI-MEM that was combined with 75.6 µg of the sgRNA libraries and 94.5 µg of lentiviral packaging mix (#CPCP-K2A, Cellecta; containing psPAX2 and pMD2 plasmids that encode Gag/Pol and VSV-G, respectively). 72h post transfection, lentivirus was harvested, aliquoted, and frozen at -80°C. Viral titer was measured using the LentiX qPCR kit (#631235, Clonetech) and was typically in the range of 5.0 $e10^6$ TU/ml.

### Pooled CRISPR screen in HCT116-Cas9

The HCT116-Cas9 clone described above was expanded to 2.0 $e10^8$ cells and transduced with the lentiviral sgRNA library (described in detail above) with a coverage of 5 sgRNAs/gene and a multiplicity of infection

of 0.5. As described above, the library was designed as two sublibraries each covering 52'000 sgRNAs. Complexity of each subpool was always kept above at least 500 cells/sgRNA. Each subpool was cultured in one CellSTACK flask (#3313, Corning) seeded with 6.7 $e10^7$ cells on day -1. On day 0 each CellSTACK was infected with one of the subpools. Five days after sgRNA infection and continuous selection on puromycin (2 μg/ml), cultures of each subpool were subcultured and divided into three CellSTACK flasks at a cell density of 3.5 $e10^7$ cells. One day later JQ1 was added at an $IC_{20}$ (0.2 μM) or $IC_{50}$ (1 μM) to both subpool cultures, the control cultures were treated with DMSO only and were used as time-matched controls for the subsequent analysis. DMSO concentration was adjusted to be equal in all cultures. Cultures were propagated and diluted again to 3.5 $e10^7$ cells when cells reached confluency (on days 8 and 12). On day 15, 7.0 $e10^7$ cells per condition were harvested and the genomic DNA was extracted using the QIAamp DNA blood maxi kit according to manufacturer's instructions (#51194, Qiagen). The purity of the pools on Day15 was assessed by flow cytometry and showed 99% RFP positive cells for both subpools.

The experiment with the minipool was conducted as described above with the exception that the complexity of the library was kept above 1000 cells/sgRNA and the screen was performed in T300 flasks (TPP, 90301) with a seeding density of 3.5 $e10^6$ per condition. In addition, cells were harvested 14 days after infection instead of 15. Genomic DNA was extracted from 5$e10^6$ cells pellets using Purelink Genomic DNA Mini Kit (K182002).

### Determination of relative sgRNA abundance

Genomic DNA was quantified using Picogreen (#P11496, Invitrogen) following the manufacturer's recommendations. Illumina sequencing libraries were generated using PCR amplification with primers specific to the genome integrated lentiviral vector backbone sequence. A total of 24 independent PCR reactions were performed per 55,000 sgRNA transduced sample. PCR reactions were performed in a volume of 100 μl, containing a final concentration of 0.5 μM of each PCR primer (Integrated DNA Technologies, 5644 5'-AATGAT ACGGCGACCACCGAGATCT ACACTCGATTTCTTGGCTTTATATATCTTGTGGAAAGGA-3' and INDEX 5'-CAAGCAGAAG ACGGCATACGAGATXXXXXXXXXXGTGACTGGAGTTCAGACGTGTGCTCTTCCGATC-3', where the Xs denote a 10 base PCR-sample specific barcode used for data demultiplexing following sequencing), 0.5 mM dNTPs (#4030, Clontech), 1x Titanium Taq DNA polymerase and buffer (#639242, Clontech). PCR cycling conditions were as follows: 1x 98°C for 5min; 28x 95°C for 15sec, 65°C for 15sec, 72°C for 30sec; 1x 72°C for 5min. The resulting Illumina libraries were purified using 1.8x SPRI AMPure XL beads (#A63882, Beckman Coulter) following the manufacturer's recommendations and qPCR quantified using primers specific to the Illumina sequences using standard methods. Illumina sequencing libraries were then pooled and sequenced with a HiSeq 2500 instrument (Illumina) with 1x 30b reads, using a custom read 1 sequencing primer 5645 (5'-TCGATTTCTTGGCTTTATATATCTTGTGGAAAGGAC GAAACACCG-3'), and a 1x 11b index read, using the standard Illumina indexing primer (5'- GATCGGAAGAGCACACGTCTGA ACTCCAGTCAC-3'), following the manufacturer's recommendations. A total of 50-60 $e10^6$ reads were generated per transduced sample, resulting in an average of approximately a 1000 reads per sgRNA.

### Screen data processing and quality analysis

Raw sequencing reads were converted to FASTQ format using Illumina bcl2fastq2 (Illumina bcl2fastq2 (Version 2.17.1.14); retrieved from http://support.illumina.com/downloads/bcl2fastq-conversion-software-v217.html). The reads were trimmed to the guide sequence using fastx-toolkit (Gordon, A and Hannon, G. FASTX Toolkit (Version 0.0.13); retrieved from http://hannonlab.cshl.edu/fastx_toolkit/index.html) and the trimmed reads were aligned to the sgRNA sequences in the plasmid library using Bowtie (Langmead et al., 2009) with no mismatches allowed.

The R software package DESeq2 (Love et al., 2014) was used to evaluate differential sgRNA representation between the compound treated and the untreated samples. A robust z-score for each sgRNA was calculated using the median and mean-absolute deviation across the log2 fold changes of the library combined results. To summarize the results at the gene level we applied a methodology derived from siRNA screening analysis named redundant siRNA activity (RSA) analysis (Konig et al., 2007). It models the probability of a gene 'hit' based on the collective activities of multiple siRNAs/sgRNAs per gene. All sgRNAs in our pool were initially ranked according to their individual signals. Then, the rank distribution of all 5 sgRNAs targeting the same gene was examined and a P-value was assigned. Thus, P-value indicates the statistical significance of all 5 sgRNAs targeting a single gene being unusually distributed toward the top (RSA up) or bottom (RSA down) ranking slots. To visualize the gene significance and result strength,

we plot the RSA up value against the Q3 z-score for each gene for the investigation of gene deletion that promotes resistance and the RSA down value against the Q1 z-score for each gene for investigating genes that upon deletion increase sensitivity to the compound treatment. We used a hypergeometric test to analyze enrichment of gene sets in our study.

### Generation of mutant clones and validation

The following gRNA sequences were cloned into the pNGx-LV-g003 lentiviral backbone (DeJesus et al., 2016) and transduced into the HCT116-Cas9 clone described above at an MOI 0.5: ATP2C1 5′- GAACTCT ATCCCCAACAGAA-3′, FERMT2 5′-GGTGGGAAAAGAAGAGAACT-3′, DUSP5 5′- GCGCTACGTGCTGCC CGACG-3′. The cells were selected for 4 days using 2 μg/ml puromycin and transduction efficiency (RFP signal) was assessed by FACS analysis. Selected cells were diluted to a density of 100-300cells / 20 ml and seeded in 15 cm dishes in puromycin containing medium. After 2 weeks, single colonies were picked using cloning discs, expanded for another 10-15 days and frozen down as master stocks.

Editing was assessed by genotyping as follows. Genomic DNA was extracted for each clone using Qiagen's QIAamp DNA mini Kit (51304) and the DNA regions across each sgRNA were amplified by PCR using Promega's GoTaqGreen master mix (M7122) following the standard protocol. The PCR bands were extracted using Zymo Research's Zymoclean Gel DNA Recovery Kit (D4001) and submitted to Sanger sequencing (Microsynth standard service). The sequences were analysed using the Vector NTI Advance (Invitrogen, version 11.5.4).

### JQ1 dose response curves

Cell growth of HCT116-WT and the different clones were compared using an imaging method to determine percentage confluency with an IncuCyte ZOOM instrument (EssenBio, Welwyn Garden City, UK) using the Basic Analyzer software of the instrument. In brief, 50,000 cells were seeded in CnT-PR (CellnTec, Bern, Switzerland) supplemented with 5% FBS, in to 6well plates and confluency measured over 72 hours. Values are displayed as phase object confluence (percent) over time.

### JQ1 dose-response curves in cation solutions

HCT116-WT (HCT116-Cas9), HCT116-ATP2C1 and HT-29 were seeded in 384well plates at a density of 750 cells/well in 40ul total volume using a Multidrop plate dispenser (Thermo Scientific) and incubated O/N at 37°C. SUM159PT were seeded at a density of 500 cells/well. The following day, 20 μl were removed from each well using a Cybio SELMA 384/60 μl semi-automated pipetting station (analytik jena) and 20 μl of $CaCl_2$ (Sigma 21097) or $MnCl_2$ (Sigma M1787) solutions were added manually according to final layout. JQ1 was then dispensed on top in a dose response manner ranging from 2.4nM-10 μM and a dilution factor of 1:2 using a TECAN D300e digital dispenser. DMSO concentration was kept at 0.2% across all conditions. 96 hours after compound addition cell viability was measured using the CellTiter-Glo assay according to the manufacturer's instructions (#G7573, Promega) using an EnVision plate reader (Perkin Elmer). Data was analyzed and $IC_{50}$ were calculated using the nonlinear regression curve fit tool (Sigmoidal, 4PL, X is log(concentration)) in GraphPad Prism (version 9.1.2).

Subtle differences in the $IC_{50}$ values measured here compared to the JQ1 dose-response described above ($IC_{50}$=0.64 vs $IC_{50}$=1 μM for screen) on HCT116-WT cells could be explained using different compound batches and were within the experimental variability expected for such experiments.

### Gene expression

The cells were lysed directly in 350 μl RLT Plus buffer including 1% β-mercaptoethanol, transferred onto a gDNA Eliminator spin column and further processed according to RNeasy Plus Mini kit (Qiagen 74134). For quantitative PCR (qPCR) analysis, a 2 μl sample RNA from each sample was processed according to the manufacturer's instructions, using KAPA SYBR Fast Once-step Universal qPCR Kit (# KK4652, KAPA). The relative expression levels of mRNA were evaluated using a real-time PCR system (Viia7, Thermo Fisher Scientific). Differences in expression levels were normalized to RPL32 as housekeeper, and the results were analyzed using the comparative Ct $2^{-\Delta\Delta Ct}$ method. Three independent biological replicates were measured in triplicates. Primers used, designed by microsynth, were as follows:

RPL32:

Forward: 5′-AAACCCAGAGGCATTGACAAC-3′

Reverse: 5′-TAACCAATGTTGGGCATCAAG-3′

ATP2C1:

Forward: 5′-GCCGTGGCTGACACTAAAGAC-3′

Reverse: 5′-TTTTGAAAACGTGCAACCTTCATTT-3′

### WES simple western protein analysis

Cells were seeded in duplicates at a density of 300′000 cells/well in 6well plates and incubated O/N at 37°C. The following day, medium was replaced and cells were treated for 24h in fresh medium containing either DMSO (0.01%), JQ1 (0.2 μM or 1μM) or JQ1 (-) (1 μM). Cells were lysed in 160 μl M-PER lysis buffer (Thermo Scientific 78503) supplemented with complete EDTA Protease inhibitor cocktail (Roche 11873580001). Protein quantification using Pierce™ BCA Protein Assay Kit (Thermo Scientific™, Cat. No. 23225) was measured after a quick centrifugation step (5 min at 9000 rpm) and samples were further diluted in 0.1X sample buffer (Protein Simple, 042-195) to a concentration of 0.7 mg/ml. Samples were analyzed on a WES® (Simple Western system) using standard reagents according to the manufacturer's instructions (Protein Simple, SM-W004). Anti ATP2C1 (Invitrogen, PA5-109430) and anti β-actin (SIGMA, A5441) primary antibodies were used at a 1:100 dilution. Default assay parameters were used for control and data analysis and peak areas were calculated using the "dropped lines" setting in the Compass software (Compass for SW Version 3.1.7, Build ID 1205). The peak area values of each sample were normalised to the corresponding untreated HCT116 from that run. Data from 5 independent runs were pooled and analyzed in GraphPad Prism (version 9.1.2).

### FURA-2 method

Intracellular Mn concentrations were measured using the CFMEA protocol as previously described (Kwakye et al., 2011). Cells were seeded in 96 well plates at the density of 20′000 cells (HCT116-Cas9) or 10′000 cells (Caco-2) in 100 μl fresh medium and allowed to attach for 5-6h. Compound was dispensed on top of the cells using a TecanD300e liquid dispenser and incubated O/N (~16 h) at 37°C. The cells were then washed once with 150 μl PBS and submitted to $MnCl_2$ supplemented medium for 6h. They were then washed 3 times with 150 μl PBS and incubated for 2h in Fura-2 (Enzo Life Sciences ENZ-52007) containing lysis buffer (PBS + 0.1% Triton-X + 0.5 μM Fura-2). Fura-2 fluorescent signal was read using an Envision plate reader (Ex360, Em535) and extracted Mn values read from the $MnCl_2$ standard curve. 20 μl of the cell lysates were then transferred to a fresh 96well plate and DNA content was then measured (Ex485, Em535) following the Quant-iT PicoGreen dsDNA Assay Kit standard protocol in 100 μl final volume (Life Technologies P11496). The extracted Mn values were normalized to DNA content to correct for differences in cell growth.

### Solvias metal ion analysis

Pellets were prepared as follows, mirroring the conditions of the CFMEA experiment described previously: $1e10^8$ HCT116-WT cells were seeded in T300 flasks for each condition (5 flasks with $2e10^7$ per condition) and allowed to attach for 5-6h. Once attached, the cells were exposed to 1 μM JQ1, 1 μM JQ1 (-) or DMSO O/N at 37°C. The cells were then washed once with PBS and submitted to fresh medium supplemented with 50 μM $MnCl_2$ (Sigma M1787) for 6h. The cells were then washed twice with PBS, harvested, pooled and $5e10^7$ cells pellets were flash frozen in an ethanol/dry ice bath. Pellets were then sent in triplicates, without annotation of conditions, for analysis by Inductively Coupled Plasma Mass Spectrometry (ICP-MS) to detect intracellular levels of Mn, Fe, Cu and Zn (Solvias, standard protocol SM37131, LOQ 0.2-2 mg/kg).

## QUANTIFICATION AND STATISTICAL ANALYSIS

Statistical significance was calculated using Two-way ANOVA with Dunnett's multiple comparison tests or unpaired T-test in the GraphPad Prism software as described in the figure legends. Values are displayed as Mean ± S.D. and the number of replicates (n value) is indicated for each figure. Statistical significance is displayed on the figures with asterisks as follows: *, $p < 0.05$; **, $p < 0.01$; ***, $p < 0.001$; ****, $p < 0.0001$; $p > 0.05$ was considered not significant.